

Is Segment Anything Model 2 All You Need for Surgery Video Segmentation? A Systematic Evaluation

Cheng Yuan^{1,*}, Jian Jiang^{1,*}, Kunyi Yang^{1,*}, Lv Wu¹, Rui Wang¹, Zi Meng¹, Haonan Ping¹, Ziyu Xu¹, Yifan Zhou¹, Wanli Song¹, Hesheng Wang¹, Qi Dou², Yutong Ban¹

Abstract—Surgery video segmentation is an important topic in the surgical AI field. It allows the AI model to understand the spatial information of a surgical scene. Meanwhile, due to the lack of annotated surgical data, surgery segmentation models suffer from limited performance. With the emergence of SAM2 model, a large foundation model for video segmentation trained on natural videos, zero-shot surgical video segmentation became more realistic but meanwhile remains to be explored. In this paper, we systematically evaluate the performance of SAM2 model in zero-shot surgery video segmentation task. We conducted experiments under different configurations, including different prompting strategies, robustness, etc. Moreover, we conducted an empirical evaluation over the performance, including 9 datasets with 17 different types of surgeries.

I. INTRODUCTION

The rapid development of the computer vision has seen foundation models demonstrating impressive zero-shot and few-shot capabilities across various tasks. Segment Anything Model (SAM) is a notable example for semantic segmentation with exceptional ability in learning general representations from large datasets of Vision Transformer (ViT) structure. It was the first foundation model released for semantic segmentation and has demonstrated promising results across various domains. However, when segmenting video data, it still requires prompts for each frame, which can be time-consuming and impractical for dynamic scenes. Recently, the Segment Anything Model 2 (SAM 2) has extended the zero-shot segmentation capabilities of the original SAM to video data. Trained on the SA-V dataset, which includes 35.5 million masks across 50.9 thousand videos, SAM 2 demonstrates robust zero-shot abilities for video segmentation. Additionally, SAM 2 incorporates a memory bank that facilitates the propagation of prompts from the first frame throughout the video. This feature makes it particularly well-suited for the surgery scene segmentation and tracking of surgical tools in surgical videos. As shown in Fig. 1, SAM2 can be generalized into many fields of surgery assistant task, such as robotic assistance and video processing in laparoscopic, gynecological, cardiac, thoracoscopic, ophthalmic, and urological surgeries. Surgery scene segmentation and surgical tool tracking are crucial tasks for understanding surgical scenes and reconstructing dynamic

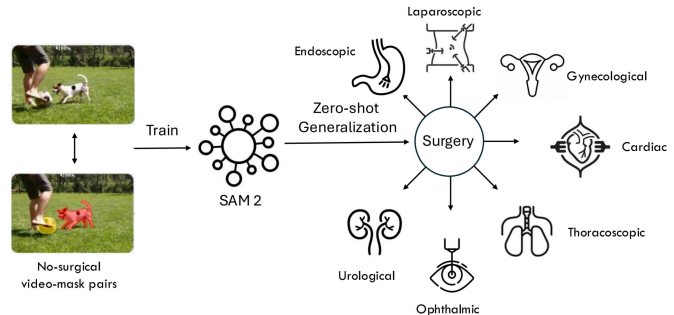


Fig. 1: Zero-shot generalization of SAM2 in Surgical Videos

surgical environments. Accurate segmentation of both surgical tools and anatomy structures are essential, but collecting pixel-level masks for each frame is resource-intensive. In this study, we not only paid attention to zero-shot segmentation performance of the SAM 2 model on different surgery types, including both laparoscopy and ophthalmoscopy, but also first evaluated different prompts influence on segmentation and tracking tasks.

II. RELATED WORKS

Artificial intelligence (AI) tools are rapidly maturing for medical applications, with many studies determining that their performance can exceed or complement human experts for specific medical use cases. Uni-modal supervised learning AI tools have been assessed extensively for medical image interpretation, especially in the field of radiology, with some success in recognizing complex patterns in imaging data. Surgery, however, remains a sector of medicine where the uptake of AI has been slower, but the potential is vast. Here, we will review the remarkable progress of AI methods in both temporal and spatial surgical tasks.

A. Surgical Temporal Task

Each surgery consists of a single procedure. A series of smooth and continuous surgeries is the accomplishment of tasks in a step-by-step manner, without interruption or stagnation, which can be divided into defined process units, known as surgical phases or steps. As for temporal-related task in surgery video, surgical phase or step recognition is the important part. Image classification using AI involves predicting what is shown in an image based on a single image. The earliest works on the analysis of surgical procedures

*Equal contribution as first author

¹Shanghai Jiao Tong University, China

²The Chinese University of Hong Kong, China

Corresponding author: yban@sjtu.edu.cn

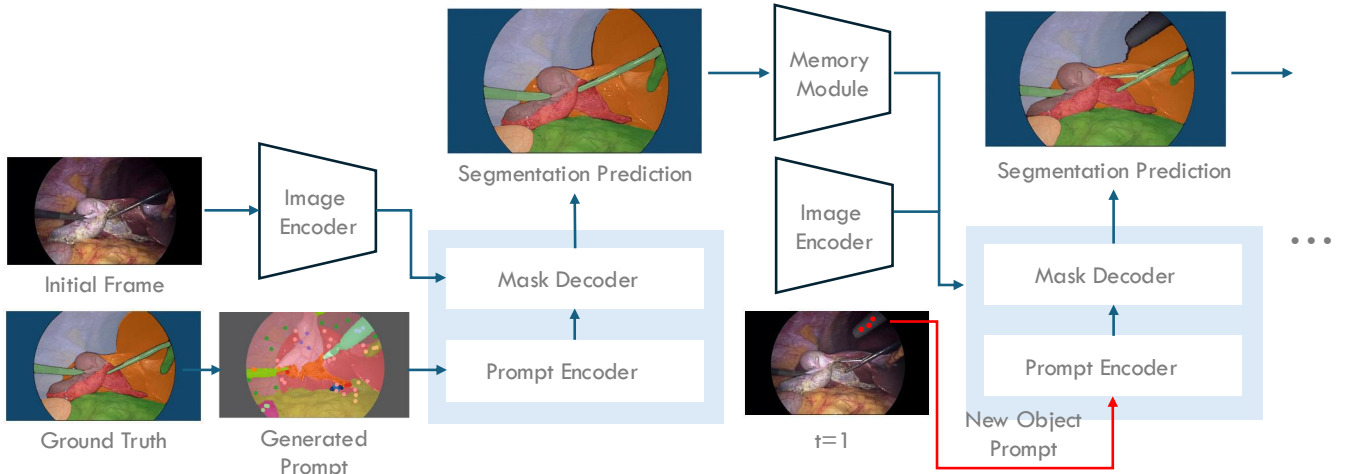


Fig. 2: The overall pipeline of SAM2 in surgery videos.

by decomposing them into sub-parts are published in 2001 by Jannin et al [19]. and MacKenzie et al. [23]. Due to the tremendous classification and recognition capabilities of multi-layer neural networks, deep learning models are used progressively in surgical recognition tasks and their potential is confirmed by many studies. In early studies, Convolutional Neural Networks (CNNs) were shown to be more effective for feature extraction than state-of-the-art statistical methods. One strategy for surgical workflow analysis is performing frame-wise classification directly based on extracted features from a single image. Zhang et al. [38] improved this approach using a 3D CNN to extract features. Pradeep and Sinha[26] extracted spatio-temporal features from 64 images together and used them for classification directly. Another strategy is based on recurrent neural network (RNN) for sequential data. Zia et al.[44] achieved the best results in their study with single-layer bi-directional RNN. Ban et al. [3], [4] uses a spatial temporal graph for a more granular understanding of surgical videos.

B. Surgical Spatial Task

In the field of spatial feature perception, instrument and anatomy segmentation is critical for surgical scene understanding, as it enables the development of computer-assisted systems for regions of interest (RoI) tracking[8], pose estimation[11], and surgical phase estimation [29]. There has been significant progress in addressing this problem. Models based on CNNs have been common for surgical RoI segmentation. Initial efforts used Fully Convolutional Networks (FCN) for instrument parts segmentation. Later, the Endoscopic Vision (Endovis) 2017 Robotic Instrument Segmentation Challenge and its 2018 version introduced the instrument sub-type segmentation task. Thus, most methods adapted FCN-based models to perform semantic segmentation of the different instruments present on each frame. Some models leverage additional priors like optical and motion flow, stereoscopic information, or saliency maps. More recent approaches have modified the original task by including weak supervision [41], domain adaptation [43], and image generation [9].

C. Foundation model in Segmentation

A foundation model is any model that is trained on broad data that can be fine-tuned to a wide range of downstream tasks. Image segmentation foundation models have revolutionized the field of image segmentation, demonstrating wide generalizability and impressive performance by training on massive amounts of data to learn general representations. Prompt engineering further improves the segmentation capability of these models. Given proper prompts as additional inputs, these models can handle various zero-shot tasks across domains and produce reliable segmentation during inference. Unlike these broad successes, medical image segmentation is often limited by issues such as expensive data acquisition and time-consuming annotation processing, resulting in a lack of massive public datasets available for training. Thus it is desirable to leverage transfer learning from the natural image domain for robust medical image segmentation.

III. BACKGROUND

The Segment Anything Model (SAM) [21] introduced a powerful foundation for promptable image segmentation, utilizing a vision transformer-based architecture to generate masks for any object in an image based on various input prompts. Building upon this foundation, SAM2 extends these capabilities to the video domain while maintaining strong performance on image tasks. Both models share a core structure consisting of an image encoder, a prompt encoder, and a mask decoder, but SAM2 introduces significant modifications to enable video processing.

SAM2's image encoder diverges from SAM by employing a Hiera encoder [28] pre-trained with Masked Autoencoder (MAE) [16]. This hierarchical encoder produces multi-scale feature embeddings for each frame, allowing for more detailed spatial information to be retained. A key difference in the image encoder design is that SAM2 removes the relative positional biases present in all of SAM's encoder layers. This change improves efficiency without sacrificing performance, as SAM2 instead adopts a simpler approach of interpolating the global positional embedding to span across windows.

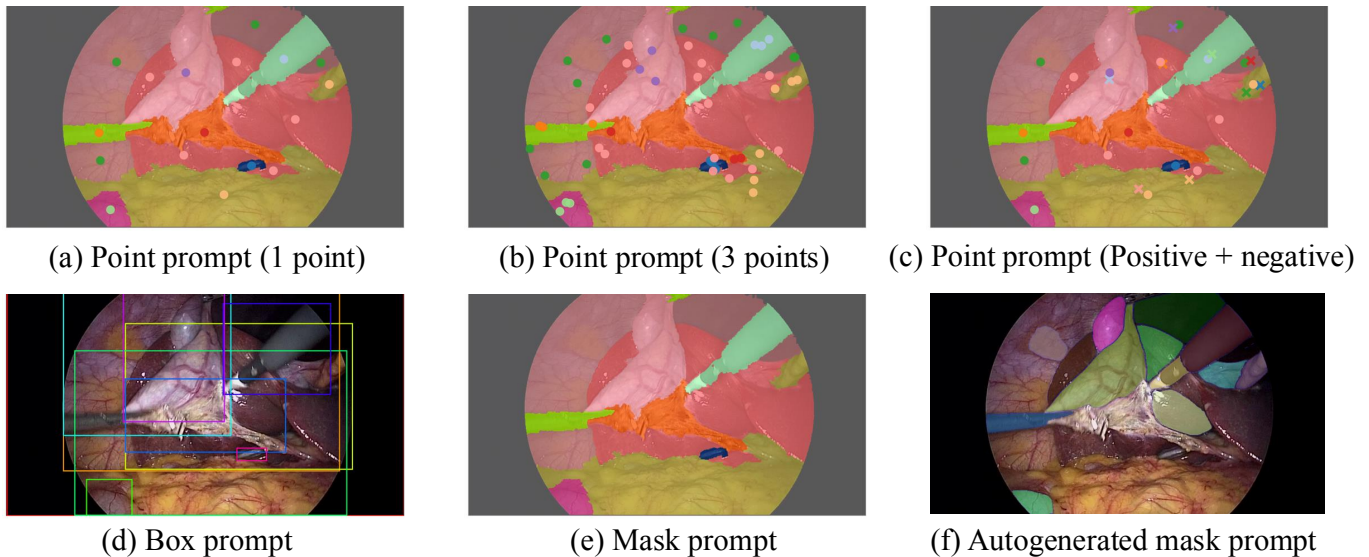


Fig. 3: Different prompting strategies evaluated in this paper.

The most substantial addition in SAM2 is the memory attention module, designed to process temporal information in videos. This module consists of stacked transformer blocks that perform self-attention on current frame features, followed by cross-attention to a memory bank. The memory bank stores information from previous frames and object pointers, utilizing 2D spatial Rotary Positional Embedding (RoPE) [17] for spatial encoding. SAM2 also introduces a memory encoder that fuses predicted mask information with image embeddings to generate memory features for future frames. While the prompt encoder remains largely unchanged, the mask decoder in SAM2 receives significant enhancements, including skip connections from the hierarchical image encoder and an occlusion prediction head. These architectural modifications enable SAM2 to effectively unify image and video segmentation within a single model, processing videos in a streaming fashion while maintaining strong performance on single-image tasks.

IV. SEGMENT ANYTHING MODEL 2 (SAM2) FOR SURGICAL VIDEO SEGMENTATION

In this section, we introduce the details of how to deploy the SAM2 model for surgical video segmentation. The re-configuration includes three major parts, different prompting strategies, re-initialization of prompts, and auto-segmentation.

A. Prompting

SAM2 supports a versatile range of prompting mechanisms, enabling users to interact with the model in various ways to specify objects of interest across video frames. The supported prompt types include points, bounding boxes, and pixel masks. Each prompt is associated with additional metadata to provide context: an object ID indicating which object category the prompt belongs to, and a frame index specifying which frame in the video sequence the prompt applies to. This flexible format enables precise guidance for object segmentation across multiple frames.

Point prompt Point prompts consist of x and y coordinates, along with additional metadata. The label value (0 or 1) distinguishes between negative and positive points, allowing users to specify both object and non-object locations. Multiple point prompts can be used for a single object, providing fine-grained control over the segmentation. In our work, since our tested datasets do not include point prompts and we are not considering human labeling, we implement a comprehensive point prompt extraction strategy. This approach involves randomly sampling points from existing box or mask prompts, with additional mechanisms to introduce controlled variability. See IV-C for details on our point extraction process.

Box prompt Bounding boxes are represented as two points, i.e., the top-left and bottom-right corners. They use special labels to distinguish them from regular point prompts: the top-left corner is labeled 2, and the bottom-right corner is labeled 3. This representation allows SAM2 to handle boxes consistently with its training on point data. While an object can only have one box prompt, it is possible to combine a box prompt with multiple additional point prompts for more precise segmentation.

Mask prompt Mask prompts provide pixel-level information about the object. They are binary masks where True indicates object pixels and False indicates background. The mask should be the same resolution as the input frame. Mask prompts are particularly useful for refining segmentations or propagating known segmentations to nearby frames. Typically, one object has one mask prompt.

The ability of SAM2 to handle prompts across multiple frames is a key feature for video segmentation tasks. Users can provide prompts on a single frame and let SAM2 propagate to other frames, or give prompts on multiple frames to guide the segmentation through challenging scenarios such as occlusions or rapid motion. This multi-frame prompting capability allows for iterative refinement of segmentations by adding prompts based on initial results.

Internally, SAM2 encodes these various prompt types into

TABLE I: All datasets evaluated in this paper. "Num. masks" refers to the number of images with non-zero mask.

Dataset name	Operation Type	Object(s) of interest	Total number of frames
Endoscapes-Seg50	laparoscopic cholecystectomy	Instruments, tissues	1933
SurgToolLoc	robotic surgery	Instruments, tissues	740850
CholecSeg8k	laparoscopic cholecystectomy	Instruments, tissues	8080
EndoNerf	DaVinci robotic prostatectomy	Instruments	219
CaDISv2	cataract surgery	Instruments, tissues	4670
Endovis17	laparoscopic surgery	Instruments	3000
Cholec80	laparoscopic cholecystectomy	Instruments, tissues	89313
Endovis18	Nephrectomy surgery	Instruments	3232
SurgicalLive24	Laparoscopic pancreatic tumor resection, Laparoscopic gastrectomy Total laparoscopic hysterectomy, L-RAMPS, Laparoscopic colon cancer, Thoracoscopic resection mediastinal tumor, Laparoscopic ovarian cystectomy, Laparoscopic right adrenalectomy, hernia repair, Transurethral resection of bladder tumor (TURBT), Ureteroscopy stone extraction	Instruments, tissues	168956

a unified representation that can be processed by its attention mechanisms. This allows the model to seamlessly integrate information from different prompt types and across multiple frames, enabling efficient and accurate segmentation across a wide range of video scenarios.

B. Initialization and Data Preparation

To process various datasets, we employ a consistent initialization strategy. Our approach handles both video clips and image datasets, supporting common formats such as jpg, png, and jpeg. For video clips, we first sample them to extract individual frames, which are then sorted in temporal order. Ground truth annotations in our tested datasets are provided in two formats: bounding boxes and masks in COCO format, or pixel-level mask images. To unify the testing process, we convert all pixel-level masks to COCO format. From these annotations, we create a set of prompts including points, masks, and bounding boxes to test the performance of SAM2 with various input types. The first frame containing ground truth annotations is selected as the initial prompt frame, denoted as I_p^0 , where p indicates that this frame is selected as a prompt frame. This approach mimics real-world scenarios with minimal expert annotation and tests the ability of SAM2 to propagate segmentation across videos.

C. Point Prompt Extraction Strategy

To evaluate the performance of SAM2 with different input types, we implement a comprehensive point prompt extraction strategy. The main reason for this approach is that our tested datasets do not have point prompts. This strategy allows us to test the model ability to segment objects accurately based on minimal input information.

Our point extraction process involves randomly sampling N positive points inside each instance-level mask or bounding box in I_p^0 . For objects with multiple mask areas due to occlusion, we sample N points for each separate area. We also generate M negative points for each area, selected from positive points of other objects. To introduce variability and

robustness in point selection, we implement a point fluctuation mechanism. This mechanism slightly adjusts the position of each selected point within a small radius, controlled by a hyperparameter beta. The fluctuation is applied in both x and y directions, with the new position clamped to ensure it remains within the image boundaries.

Additionally, we consider a center point (the center of the box for bounding boxes, or the center of mass for masks) as a special prompt. This strategy allows us to test the performance of SAM2 with varying levels of input information, from sparse point sets to more comprehensive representations of object boundaries.

D. Re-initialization Strategy

Based on preliminary results, we found that using only the first valid frame I_p^0 may not be sufficient to guide a long video clip. This is because I_p^0 may not contain all objects of interest, and some objects may temporarily disappear and reappear, challenging the tracking ability of SAM2. To address these issues, we implement a re-initialization strategy that can be triggered in two cases. The first case is every T frames, where T is a predefined interval. The second case occurs when a new object not present in the current prompt frame comes into consideration. These re-initialization cases can be applied together or separately, depending on the specific requirements of the video sequence being processed. The re-initialization process involves finding a new prompt frame I_p^t and discarding the previous prompt frame, extracting object information (including identifying prompt objects, building a SAM2 video predictor, and initializing the inference state), and reinitializing the SAM2 predictor. This approach helps maintain tracking accuracy over longer video sequences and adapts to changing scene conditions. By not using previous prompts, we allow the model to focus on current information and avoid incorrect segmentation of old objects that may no longer be relevant.

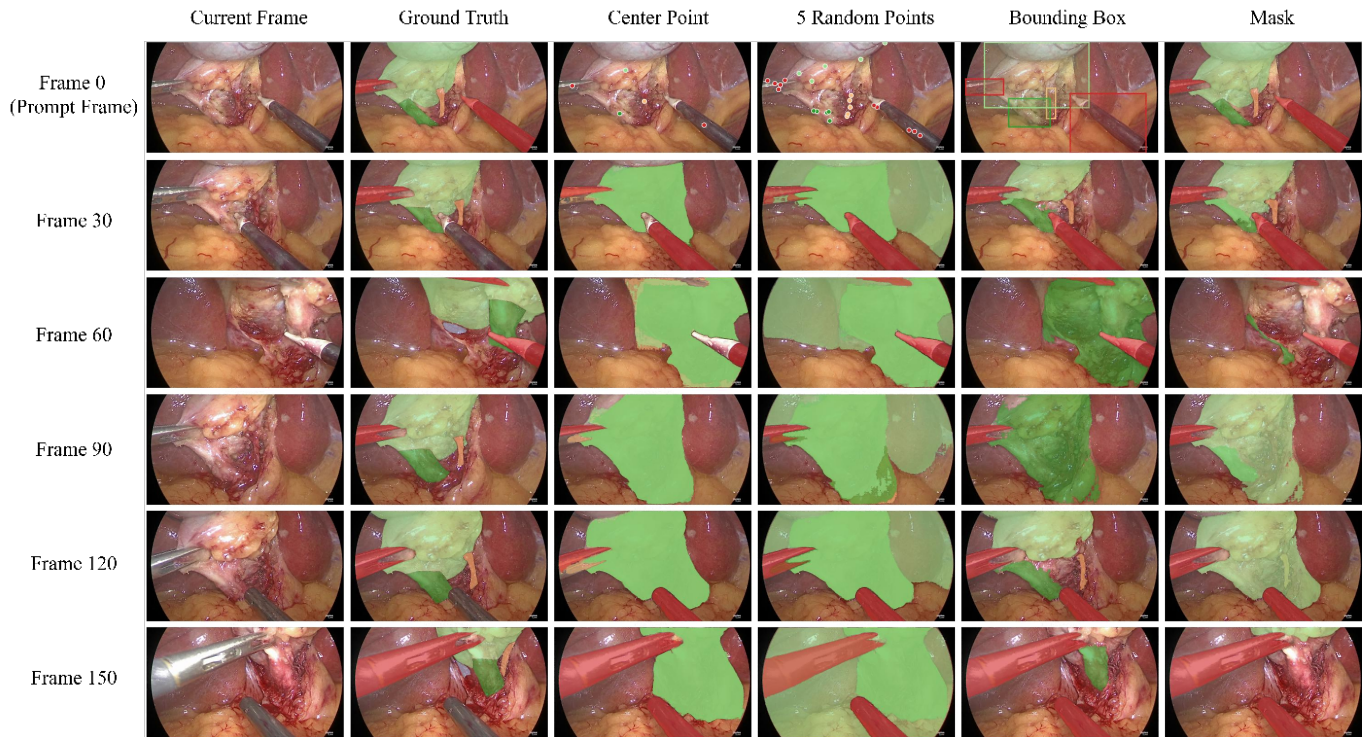


Fig. 4: Segmentation Results on Endoscopes-Seg50 Dataset.

E. Prompt Perturbation Strategy

To further assess the robustness of SAM2, we implement a prompt perturbation strategy for both bounding boxes and masks. The primary reasons for introducing this strategy are to simulate real-world scenarios where annotations may be imperfect or subject to variation, to test the model ability to handle input perturbations and maintain accurate segmentation, and to evaluate the performance limits of SAM2 under challenging conditions. Our perturbation strategy includes applying random shifting and scaling (50% to 150% of the original size) for bounding boxes, and implementing translation, scaling, dilation, erosion, and affine transformation for masks. By introducing these controlled perturbations, we can systematically evaluate the resilience of SAM2 to input noise and its ability to maintain accurate segmentation under various levels of input uncertainty.

F. Auto-segmentation for Unannotated Datasets

For datasets lacking ground truth annotations, we utilize the auto mask generation techniques provided by SAM2 to automatically generate pseudo ground truth for the first frame. Our preliminary results indicate that segmentation quality is highly sensitive to certain hyperparameters. Thus, we perform an extensive hyperparameter search to find optimal settings for datasets without ground truth.

Key hyperparameters in our auto-segmentation process include the number of points sampled per side of the image, which influences the likelihood of capturing all objects, and the predicted mask quality threshold. We also consider stability score thresholds and offsets, which affect the robustness of mask generation. The non-maximal suppression threshold for filtering duplicate masks and the minimum mask region area

for post-processing are crucial for refining the generated masks. Additionally, we explore the impact of multi-scale processing through crop layers and the use of mask-to-mask refinement.

The final hyperparameters for auto segmentation are chosen based on expert visual inspection, considering factors such as mask completeness, boundary accuracy, and the ability to distinguish between close or overlapping objects. This process ensures that the generated pseudo ground truth is of high quality and suitable for further processing and evaluation.

For a detailed list and description of the hyperparameters used in our auto-segmentation process, see V.

V. EXPERIMENTS

A. Dataset

In this work, we systematically evaluated on series of public and in-house datasets. An overview of the datasets used can be found in Table I. The detailed description of the datasets is as follows:

EndoVis2018 The EndoVis2018 dataset was introduced as part of the 2018 MICCAI Robotic Scene Segmentation Challenge. It consists of 19 videos, divided into 15 for training (2235 frames) and 4 for testing (997 frames). Each frame has a resolution of 1280×1024 and is annotated by pixel. The dataset includes 7 object categories: Bipolar Forceps (BF), Prograsp Forceps (PF), Large Needle Driver (LND), Vessel Sealer (VS), Suction Instrument (SI), Clip Applier (CA), and Ultrasound Probe (UP).

Endoscopes-Seg50 Endoscopes-Seg50 is a subset of Endoscopes2023, a dataset of laparoscopic cholecystectomy videos designed for surgical scene understanding and Critical

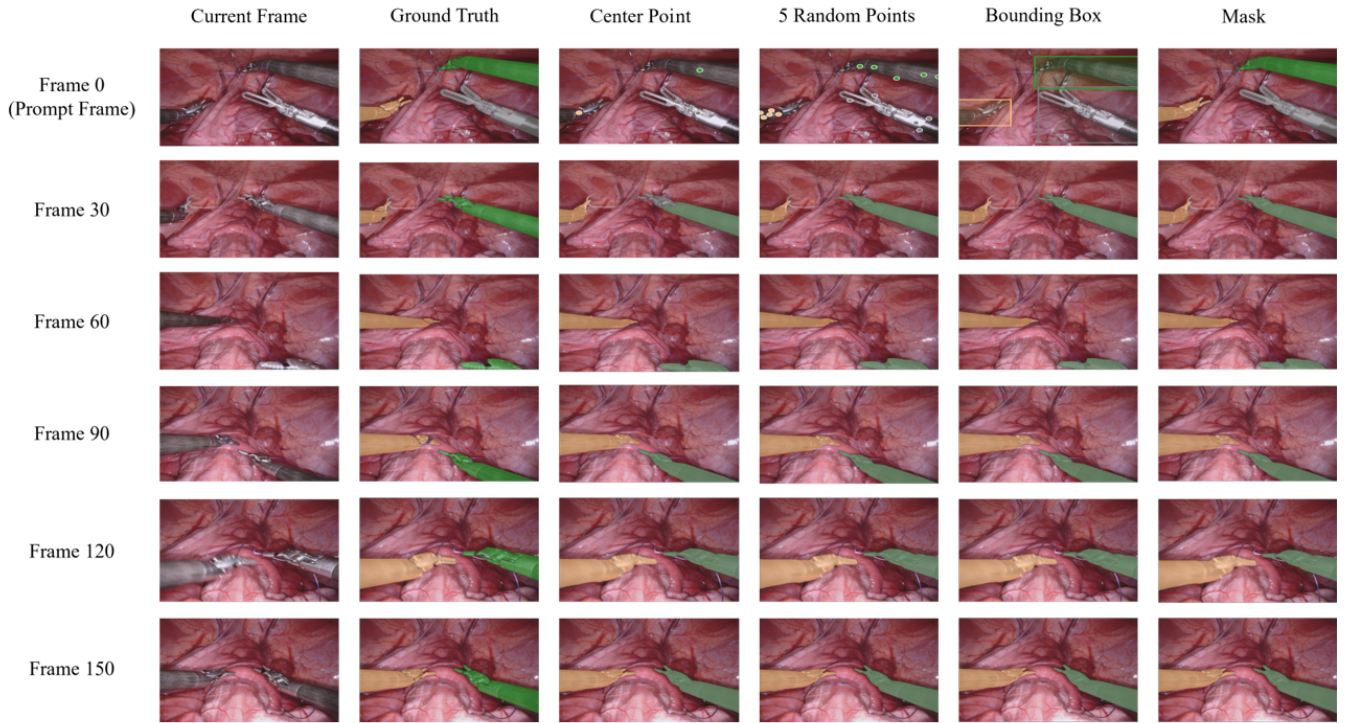


Fig. 5: Visualization of segmentation results in the EndoVis17 dataset.

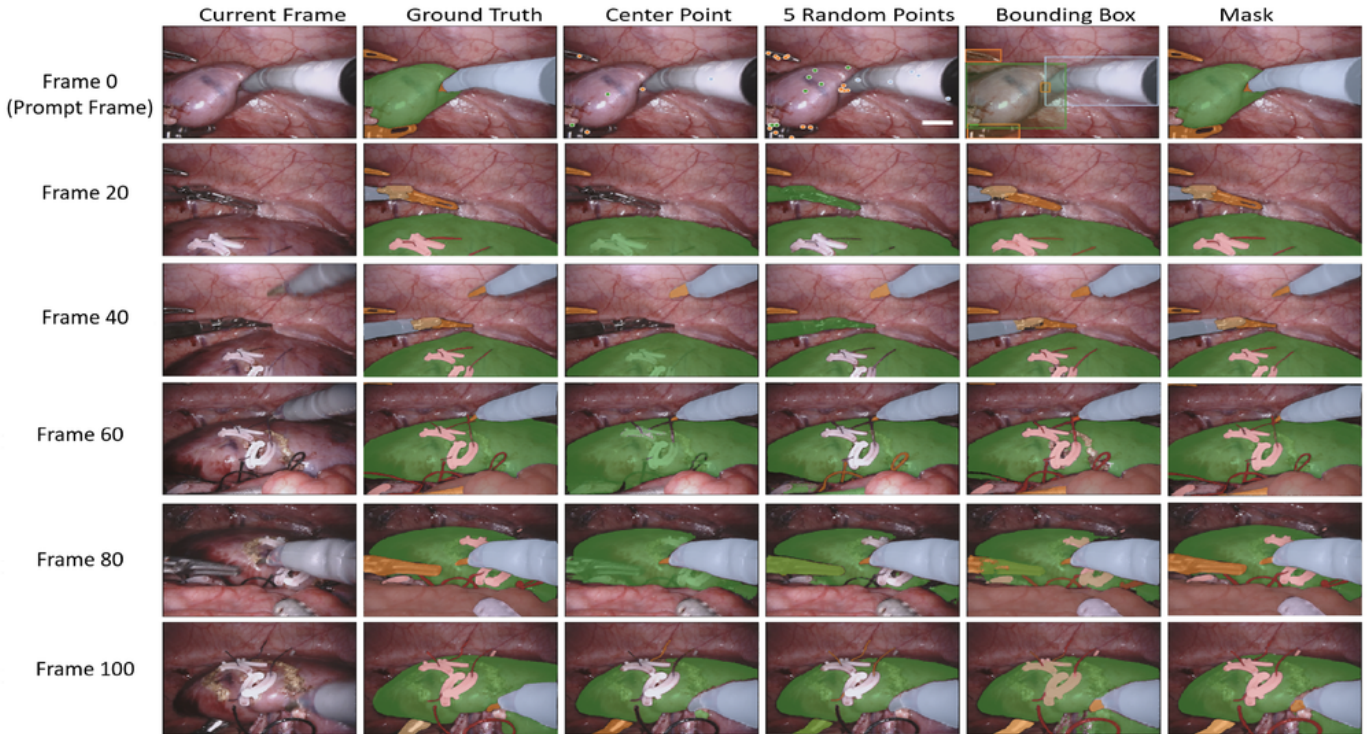


Fig. 6: Visualization of segmentation results on the EndoVis18 dataset.

View of Safety (CVS) assessment. Endoscapes-Seg50 contains 14940 frames from 50 videos. Of these, 493 frames are densely annotated with segmentation masks for 6 classes: 5 anatomical structures (cystic plate, cystic duct, cystic artery,

gallbladder, hepatocystic triangle) and surgical tools.

EndoNerf The EndoNerf dataset, consisting of two video types ("Cutting Tissues Twice" and "Pulling Tissues"),

exhibited high performance as well. For the Cutting video, SAM2 achieved a mDice of 98.32% and a mIoU of 96.71%, while the Pulling video reached a mDice of 96.09% and a mIoU of 92.87% (Tables IV). While direct comparisons with other methods are not available for this dataset, these results represent a new benchmark for performance on EndoNerf.

SurgToolLoc dataset The SurgToolLoc dataset consists of 24,695 endoscopic videos, each 30 seconds long and captured at 60 fps with a resolution of 720p (1280 x 720). The original videos, where standard activities such as dissecting and suturing are performed, are downsampled to 1 fps for processing. Fourteen possible surgical tools include needle drivers, force bipolars and so forth.

CaDIS The CaDIS (Cataract Dataset for Image Segmentation) is a dataset specifically designed for semantic segmentation of cataract surgery videos. It includes 4670 microscope images from cataract surgeries, each annotated at the pixel level to identify anatomical structures and surgical instruments. The training set consists of 25 videos, each with an average duration of about 10 minutes and 56 seconds, recorded at a rate of 30 frames per second.

Cholec80 Cholec80 is a laparoscopic video dataset containing 80 high-resolution videos, with an average duration of 39 minutes at 25 frames per second (fps). In our work, we downsampled all the original video to 1 fps for processing. The whole dataset is labeled with the phase and tool presence annotations, which a senior surgeon in Strasbourg Hospital, France defines.

CholecSeg8k CholecSeg8k consists of 17 video clips, extracted from the Cholec80 dataset, and is divided into 101 directories, each containing 80 frames, each with a resolution of 854×480 . The dataset features 13 distinct categories representing various medical instruments and anatomical structures within the surgical scene. For each frame, three types of masks are provided: a color mask, an annotation mask, and a watershed mask. The color mask visualizes classes, the annotation mask is hand-drawn for labeling, and the watershed mask simplifies class identification using pixel values for easier processing.

SurgicalLive24 The surgical dataset represents a diverse collection of surgical videos encompassing various surgical procedures, including thoracoscopy, laparoscopy, and urethroscopy. The dataset contains 11 different operations of each type of surgery. The surgery videos are sampled at 1 FPS and contains a total of 168956 frames.

B. Evaluation Metrics

To evaluate the performance of our model, we use three common metrics: **Mean Intersection over Union (mIoU)**, **Mean Dice Coefficient (mDice)**, and **Mean Absolute Error (MAE)**.

Mean Intersection over Union (mIoU): Mean Intersection over Union (mIoU) measures the average overlap between the

predicted segmentation and the ground truth across all classes. It is calculated using the following formula:

$$\text{mIoU} = \frac{1}{C} \sum_{i=1}^C \frac{\text{TP}_i}{\text{TP}_i + \text{FP}_i + \text{FN}_i}$$

Where:

- C is the number of classes.
- **TP (True Positives)** are the correctly predicted positive pixels for class i .
- **FP (False Positives)** are the incorrectly predicted positive pixels for class i .
- **FN (False Negatives)** are the incorrectly predicted negative pixels for class i .

Mean Dice Coefficient (mDice): The Mean Dice Coefficient (mDice) measures the average similarity between the predicted and ground truth segmentations across all classes. It is calculated as follows:

$$\text{mDice} = \frac{1}{C} \sum_{i=1}^C \frac{2 \times \text{TP}_i}{2 \times \text{TP}_i + \text{FP}_i + \text{FN}_i}$$

Where:

- C is the number of classes.
- **TP (True Positives)** are the correctly predicted positive pixels for class i .
- **FP (False Positives)** are the incorrectly predicted positive pixels for class i .
- **FN (False Negatives)** are the incorrectly predicted negative pixels for class i .

Mean Absolute Error (MAE): Mean Absolute Error (MAE) measures the average absolute difference between the predicted and ground truth values across all pixels. It is calculated as follows:

$$\text{MAE} = \frac{1}{N} \sum_{i=1}^N |y_i - \hat{y}_i|$$

Where:

- N is the total number of pixels.
- y_i is the ground truth value for pixel i .
- \hat{y}_i is the predicted value for pixel i .

C. Instrument Segmentation in Laparoscopic and Endoscopic Surgeries

We employ the SAM2 model to analyze three datasets used for surgical tool tracking: EndoVis17, EndoVis2018, and EndoNerf. Various prompting strategies were evaluated, including point prompts (center and random), bounding box prompts, and mask prompts. We investigated the impact of re-initialization at different intervals (5, 10, 30, and 60 frames) and also conducted experiments involving noise.

Overall Performance Segmentation quantitative results are presented in Table II III and IV, including comparisons to baseline performances from state-of-the-art (SOTA) models. Based on these results, the SAM2 model demonstrated superior performance across the EndoVis17, EndoVis2018, and

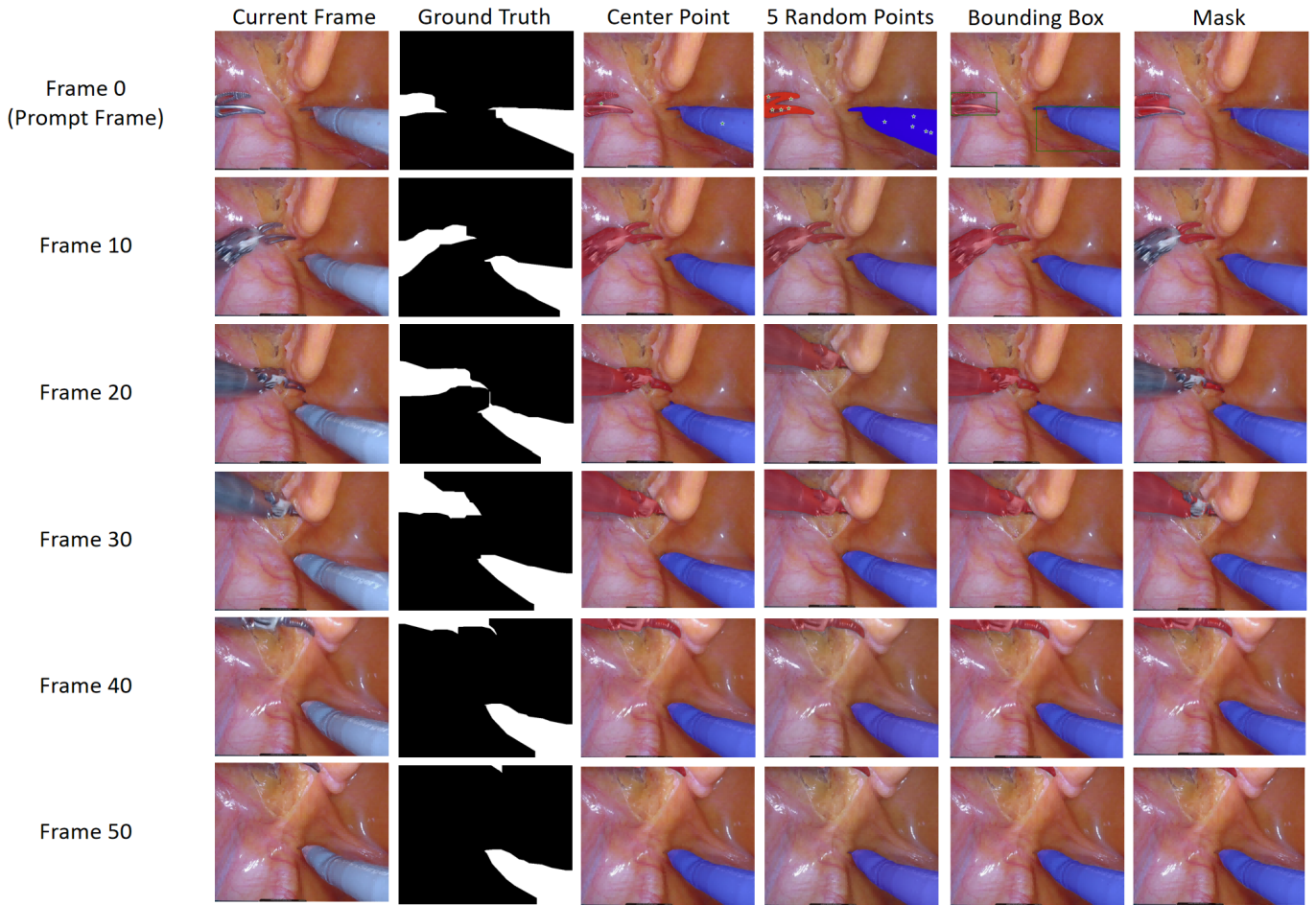


Fig. 7: Visualization of segmentation results on the EndoNerf dataset.

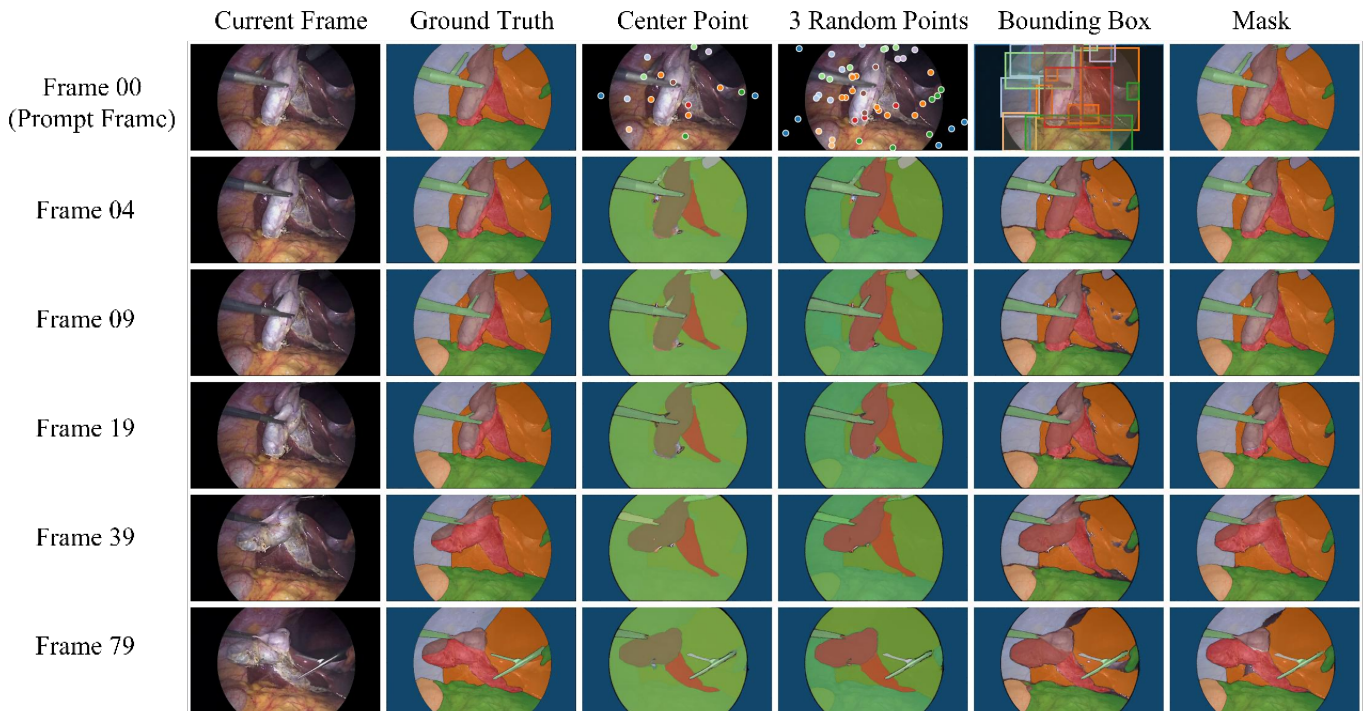


Fig. 8: Visualization of segmentation results on the CholecSeg8k dataset.

EndoNerf datasets, consistently outperforming existing state-of-the-art methods.

Mask prompts with 5-frame re-initialization generally achieved the best results. For Endovis17 (see Table II), this setting yielded an mDice of 90.73% and an mIoU of 88.04%, surpassing Surgical-DeSAM’s performance (mDice of 89.62% and mIoU of 82.41%). On EndoVis2018 (see Table III), the same configuration produced a Challenging IoU (Ch. IOU) of 82.12% and a Mean Class IoU (MC. IoU) of 80.84%, significantly improving upon the SOTA method QPN [10] (Ch. IOU of 77.77% and MC. IoU of 43.84%). In the EndoVis2018 dataset, SAM2 with mask prompts and 5-frame re-initialization excelled in segmenting challenging instrument classes, with IoU scores of 57.78% for the Large Needle Driver (LND) and 69.11% for the Clip Applier (CA), compared to QPN’s 19.96% and 0.00% respectively. For the EndoNerf dataset (see Table IV), the results varied between the two video types. In the ‘Cutting’ video, the mask prompts with 5-frame re-initialization achieved 98.97% mDice and 97.97% mIoU. For the more challenging ‘Pulling’ video, this setting reached 96.09% mDice and 92.87% mIoU.

The superiority of mask prompts was consistent across datasets, with some nuances in dynamic scenarios. For EndoVis17, at the 5-frame re-initialization setting, mask prompts (90.73% mDice) showed substantial improvement over bounding box prompts (88.11% mDice) and point prompts (83.79% mDice for random 3 points). In EndoVis2018, mask prompts (82.12% Ch. IOU) outperformed bounding box prompts (74.82% Ch. IOU) and point prompts (55.48% Ch. IOU for random 3 points). However, the EndoNerf ‘Pulling’ video presented an interesting case. Without re-initialization, mask prompts initially underperformed (79.08% mDice) compared to point prompts (90.56% mDice) and bounding box prompts (90.41% mDice). This underscores the challenge of maintaining accurate segmentation in dynamic surgical scenarios.

Effectiveness of Re-initialization re-initialization emerged as a crucial factor in maintaining high performance, particularly in dynamic scenes. For Endovis17, increasing re-initialization frequency from 60 frames to 5 frames boosted mask prompt performance from 68.55% to 88.04% mDice, with performance dropping to 55.52% mDice without re-initialization. In EndoVis2018, this change improved mask prompt performance from 67.58% to 82.12% Ch. IOU. The impact of re-initialization was most pronounced in the EndoNerf dataset. In the ‘Cutting’ video, mask prompt performance improved modestly from 98.40% mDice without re-initialization to 98.97% mDice with 5-frame re-initialization. The ‘Pulling’ video showed a dramatic improvement from 79.08% mDice to 96.09% mDice. The differential impact of re-initialization on various prompt types is noteworthy. In EndoVis2018, bounding box prompts improved from 60.52% Ch. IOU without re-initialization to 74.82% Ch. IOU with 5-frame re-initialization. This suggests that detailed initial segmentation, while valuable, can become a liability in dynamic scenes if not regularly refreshed.

Robustness to Noise The noise analysis conducted on the EndoNerf dataset provided crucial insights into the model’s robustness as shown in Table V. Both the ‘Cutting’ and ‘Pulling’ videos demonstrated decreasing mDice and mIoU scores with increasing noise levels, but with varying sensitivi-

ties. The ‘Cutting’ video showed resilience to moderate noise levels, with significant performance degradation only at higher noise levels. For instance, with a noise level of 0.1 shift and 0.3 scale, the ‘Cutting’ video maintained a high mDice of 92.78% and mIoU of 86.88%. However, when noise levels increased to 0.2 shift and 0.5 scale, performance dropped more substantially to 66.86% mDice and 50.46% mIoU. In contrast, the ‘Pulling’ video exhibited greater sensitivity, with noticeable performance drops even at lower noise levels. At a noise level of 0.05 shift and 0.1 scale, the ‘Pulling’ video’s mDice decreased to 65.81% and mIoU to 58.96%, compared to 90.41% mDice and 83.98% mIoU without noise. The performance degradation was more severe at higher noise levels, with mDice falling to 52.01% and mIoU to 48.31% at 0.1 shift and 0.3 scale noise.

Interestingly, when testing mask noise influence in the ‘Pulling’ video, we observed an unexpected behavior. The mDice and mIoU scores initially increased before decreasing as noise levels rose. For example, with a mask noise level of 0.1, the mDice improved slightly to 87.12% from the baseline of 79.08%, before declining at higher noise levels. This unexpected improvement might be due to the erosion of the mask when separating ground truths, potentially enhancing segmentation in some cases before higher noise levels negatively impacted performance.

These findings highlight the differential impact of noise on surgical tool tracking in static versus dynamic scenarios. The ‘Cutting’ video’s resilience to moderate noise suggests that in relatively stable surgical environments, the model can maintain accurate segmentation even in the presence of some visual disturbances. However, the ‘Pulling’ video’s sensitivity to noise underscores the challenges of maintaining accurate segmentation in more dynamic surgical scenarios, where even small perturbations can significantly affect performance.

D. Joint Instrument and Tissue Segmentation in Laparoscopic Surgeries

Overall Performance The performance of SAM for our five prompting modes, introduced in the Methodology, of use is shown here. As for two included datasets, there are several general conclusions. First, SAM2 performance varies widely across different datasets. It ranges from an impressive mean IoU of 98.91% to a very poor mean IoU of 20.76%. Second, comparing the performance for different prompting modes shows general superiority of mask prompts over both box and point prompts. As expected, the segmentation results of more point prompts are generally superior to those where only one point is indicated. Moreover, with different re-initialization strategies, the best performance was consistently achieved using mask prompts with 5-frame re-initialization.

Separate Segmentation Performance As for semantic segmentation, the dataset named Cholecseg8k is included in this study. *Table III* describes the quantitative segmentation performance on the Cholecseg8k. SAM2 achieved generally best performance on both instruments and tissue appeared in the whole surgery field. Using SAM2 with bounding box prompting or mask prompting can have much better segmentation outcome compared with baseline models. Furthermore,

TABLE II: Quantitative Evaluation of Instrument Segmentation on Endovis17 dataset (Numbers in %).

Method	re-initialization	mIoU	mDice
TernausNet [18]	-	35.27	-
MF-TAPNet [20]	-	37.35	-
Dual-MF [41]	-	45.80	56.12
TrackFormer [24]	-	54.91	59.72
ISINet [14]	-	55.61	62.8
TraSeTR [42]	-	60.40	65.21
S3Net(+MaskRCNN) [1]	-	72.54	-
Surgical-DeSAM [30]	-	82.41	89.62
<hr/>			
SAM2-Points-Center(Standard)	-	46.67	50.81
SAM2-Points-Center	30 frames	65.01	70.30
SAM2-Points-Center	10 frames	70.62	76.76
SAM2-Points-Center	5 frames	72.80	79.15
SAM2-Points-Random 1(Standard)	-	43.65	47.51
SAM2-Points-Random 1	60 frames	47.09	50.81
SAM2-Points-Random 1	30 frames	62.51	68.20
SAM2-Points-Random 1	10 frames	67.27	73.67
SAM2-Points-Random 1	5 frames	76.15	79.31
SAM2-Points-Random 3(Standard)	-	49.71	53.34
SAM2-Points-Random 3	60 frames	63.05	67.58
SAM2-Points-Random 3	30 frames	69.53	74.56
SAM2-Points-Random 3	10 frames	75.91	81.57
SAM2-Points-Random 3	5 frames	77.86	83.79
SAM2-Points-Random 5	-	48.96	52.67
<hr/>			
SAM2-Bbox (Standard)	-	50.44	53.67
SAM2-Bbox	60 frames	65.21	69.28
SAM2-Bbox	30 frames	73.27	77.29
SAM2-Bbox	10 frames	81.31	85.60
SAM2-Bbox	5 frames	83.74	88.11
<hr/>			
SAM2-Mask (Standard)	-	52.63	55.52
SAM2-Mask	60 frames	68.55	71.91
SAM2-Mask	30 frames	76.15	79.31
SAM2-Mask	10 frames	84.71	87.70
SAM2-Mask	5 frames	88.04	90.73

we assessed the impact of re-initialization at the interval of 60, 30, 10, and 5 frames for each method. Additionally, we tested mask and bounding box prompts with slight positional inaccuracies. The results indicate that SAM2 maintains strong segmentation performance even with these imperfect prompts, demonstrating its robustness.

Fig. 8 presents the performance of SAM2 with various prompting strategies across an example video sequence. The initial prompt frame, ground truth, and segmentation results for the four types of prompts (center point, three random points, bounding box, and mask) are displayed in the first row. The subsequent rows display these results at frames 4, 9, 19, 39, and 79, respectively. While SAM2 successfully segments and tracks surgical tools throughout the sequence, its performance on anatomical structures differs based on the prompting strategy used. Point prompting struggles to segment multiple objects of the same category within a single frame, failing to differentiate between the objects and surrounding regions. In contrast, both bounding box and mask prompting effectively mitigate this issue, providing improved segmentation of surgical tools and anatomical structures. However, mask prompting offers more precise boundary handling, whereas bounding box prompting leaves blank areas, resulting in slightly less accurate boundary segmentation.

As for instance segmentation, the dataset named Endoscapes2023 is included here. Table IV shows that using full

masks as guides worked best for image segmentation, better than using boxes or points. The model easily tracked tools, even when they moved out of and back into view. However, it struggled to find organs or tissues once they were out of view. It’s worth noting that even with slightly inaccurate masks or boxes, SAM2 still did well, showing it can handle some errors. The results show that detailed shape information is key for good segmentation, especially for organs and tissues, and that using masks or bounding box as guides is a promising approach.

Fig. 5 presents a 6x6 grid illustrating the performance of SAM2 with different prompting strategies across a surgical video sequence. The first row displays the initial prompt frame, ground truth, and segmentation generated by various prompt types (center point, 5 random points, bounding box, and mask). Subsequent rows show the these results of the 30, 60, 90, 120, and 150 frame, respectively. While SAM2 effectively segments and tracks surgical tools across the sequence, its performance on anatomic structures varies depending on different prompting strategies. Point prompts struggle with small tissues and often generate larger mask than ground truth. However, increasing the number of prompting points exacerbate mask expansion. Bounding box and mask prompts show better accuracy on small structure such as cystic artery in Frame 30. Notably, SAM2 can achieve good results when the scene reverts to a state similar to the prompt frame, as seen in Frame 120. The presence of surgical tools also appears to improve segmentation performance, as observed in the transition from Frame 90 to Frame 120.

Effect of Re-initialization The effect of re-initialization varied across the different prompting methods. In general, introducing periodic re-initialization significantly improves SAM2’s performance for mask and bounding box prompting strategies. In the Cholecseg8k dataset, every 30-frame re-initialization with bounding box prompts leads to an improvement in mIoU from 38.94% to 76.82% and mDice from 44.88% to 85.87%. Similarly, mask prompts with 30-frame re-initialization achieve mIoU of 98.91% and mDice of 99.45%, indicating the effectiveness of updated information in time and potential drift over longer video sequences. In the Endoscapes2023, the higher the IoU and Dice for the standard prompting method, the more pronounced the effect of re-initialization. For point prompting, re-initialization had minimal impact on the performance of both center point and single random point prompts, with less than a 1% change in IoU and Dice. However, for three random points, re-initialization slightly improved segmentation, increasing IoU from 0.7124 to 0.7348 and Dice from 0.7917 to 0.8130. In comparison, re-initialization had a more substantial effect on bounding box and mask prompting, with shorter re-initialization intervals leading to greater improvements. The IoU and Dice of bounding box prompting improved from 0.8334 to 0.8650 and from 0.8900 to 0.9190, respectively, while mask prompting saw its IoU increase from 0.8895 to 0.9393 and its Dice from 0.9273 to 0.9648.

Robustness to Noise Perturbation Introducing noise (scale, shift, etc.) into the initial prompts shows that SAM2’s performance can be significantly influenced by the quality of the prompts. As expected, these noise significantly impact its

TABLE III: Quantitative Evaluation of Instrument Segmentation on Endovis18 Dataset. (Numbers in %)

Method	Reinitialize	Instrument Classes IOU							Ch. IOU	ISI. IOU	MC. IOU
		BF	PF	LND	SI	CA	MCS	UP			
SimCaL [31]	-	73.67	40.35	5.57	0.00	0.00	89.84	0.00	68.56	67.58	29.92
CondInst [7]	-	77.42	37.43	7.77	43.62	0.00	87.8	0.00	72.27	71.55	36.29
BMaskRCNN [34]	-	70.04	28.91	9.97	45.01	4.28	86.73	3.31	68.94	67.23	35.46
ISINET [14]	-	73.83	48.61	30.98	37.68	0.00	88.16	2.16	73.03	70.97	40.21
SCNet [32]	-	78.40	47.97	5.22	29.52	0.00	86.69	0.00	71.74	70.99	35.40
MFTA [33]	-	71.00	31.62	3.93	43.48	9.90	87.77	3.86	69.20	67.97	35.94
Detectors [27]	-	73.94	46.85	0.00	0.00	0.00	79.92	0.00	66.69	65.06	28.67
Orienmask [13]	-	68.95	38.66	0.00	31.25	0.00	91.21	0.00	67.69	66.77	32.87
QueryInst [12]	-	74.13	31.68	2.30	0.00	0.00	87.28	0.00	66.44	65.82	27.91
FASA [37]	-	72.82	37.64	5.62	0.00	0.00	89.02	1.03	68.31	66.84	29.45
Mask2Former [6]	-	69.35	24.13	0.00	0.00	0.00	89.96	10.29	65.47	64.69	27.67
TraSeTR* [42]	-	76.30	53.30	46.5	40.6	13.90	86.3	17.5	76.20	75.60	47.77
S3Net [2]	-	77.22	50.87	19.83	50.59	0.00	92.12	7.44	75.81	74.02	42.58
Mask DINO [39]	-	82.35	57.67	0.83	60.46	0.00	90.73	0.00	75.63	76.39	41.73
QPN [10]	-	82.8	60.94	19.96	49.70	0.00	93.93	0.00	77.77	78.43	43.84
SAM2-Points-Center	-	61.34	37.75	0.00	80.07	68.25	48.39	70.45	50.80	50.80	56.76
SAM2-Points-Center	30 frames	58.02	44.65	0.00	0.00	69.44	40.16	72.24	53.96	53.96	57.02
SAM2-Points-Random 1	-	44.74	36.39	0.00	0.00	93.69	36.92	0.00	40.75	40.75	47.47
SAM2-Points-Random 1	60 frames	68.00	47.06	0.00	81.44	58.09	35.81	63.9	55.54	55.54	57.23
SAM2-Points-Random 1	30 frames	48.96	40.36	0.00	0.00	86.02	33.29	0	50.09	50.09	54.40
SAM2-Points-Random 3	-	67.43	45.93	0.00	81.58	85.19	44.52	61.93	55.48	55.48	60.71
SAM2-Points-Random 3	60 frames	66.63	43.89	0.00	77.10	74.94	21.70	69.02	50.69	50.69	52.78
SAM2-Points-Random 3	30 frames	67.96	37.55	0.00	77.17	58.39	25.76	69.67	48.35	48.35	50.59
SAM2-Points-Random 5	-	53.43	34.0	0.00	0.00	85.89	47.28	73.27	47.15	47.15	53.59
SAM2-Bbox (standard)	-	65.51	47.41	0.00	0.00	58.61	84.50	0.00	60.52	60.52	64.82
SAM2-Bbox	60 frames	70.14	49.24	0.00	0.00	49.02	83.72	82.96	62.70	62.70	64.83
SAM2-Bbox	30 frames	81.35	54.69	0.00	87.40	44.25	83.25	82.23	69.17	69.17	71.22
SAM2-Bbox	10 frames	81.11	60.74	23.49	86.63	55.96	86.95	81.67	71.26	71.26	68.46
SAM2-Bbox	5 frames	84.10	68.66	52.10	84.82	47.73	87.60	83.26	74.82	74.82	73.26
SAM2-Mask (standard)	-	66.81	46.24	0.00	0.00	51.22	85.02	0.00	57.68	57.68	60.10
SAM2-Mask	60 frames	73.49	55.82	0.00	0.00	44.54	84.76	84.95	67.58	67.58	68.63
SAM2-Mask	30 frames	80.19	60.99	0.00	85.99	56.66	87.75	83.24	73.06	73.06	75.79
SAM2-Mask	10 frames	86.75	72.10	0.00	89.12	63.47	89.75	85.50	79.67	79.67	80.12
SAM2-Mask	5 frames	86.47	76.00	57.78	90.48	69.11	92.05	88.17	82.12	82.12	80.84

performance compared to using accurate instructions. In Fig 6, adding noise to the prompt will have significant influence on the accuracy of the segmentation performance. For bounding box prompting, the IoU and Dice decrease from 0.8334 to 0.4544 and from 0.8900 to 0.5128. For mask prompting, the IoU and Dice decrease from 0.8895 to 0.4836 and 0.9273 to 0.5523. These results indicated the importance of providing SAM2 with clear and accurate guidance to achieve optimal segmentation results.

E. Results on Cataract Surgery

For cataract surgery, we conducted scene segmentation experiments on the CaDIS dataset. In the CaDIS dataset, the segmentation task was divided into 3 different subtasks, where task I focuses on the segmentation of 8 classes, task II for 17 classes, and task III for 25 classes. The qualitative evaluation of SAM2 in task I is shown in Figure 9. We observe that due to the properties of the cataract surgery video, the segmentation results from different prompts have a huge variation. Cataract surgery mainly involves eye-related tissues, often of a circular shape. First of all, due to this special scene property, the segmentation result of using one center point as the prompt is very poor, the model can barely segment the circular structure.

When adding more points as the prompt for each class, the model can segment the large areas like the cornea (colored in orange). However, it still suffers from classes like iris (colored in green). The model tends to have a robust segmentation when using bounding box and mask prompts, most of the main structures can be segmented accurately, with Frame 0 to Frame 120. However, SAM2 still has trouble with long-term tracking. When the surgical tool goes out of the scene and then comes back at Frame 150, the model cannot recover the segmentation mask for the tool.

The quantitative evaluation of the CaDIS dataset is shown in Table VIII, we observe that the zero-shot segmentation of SAM2 does not outperform the existing method in Task I. Existing methods are trained on the dataset already. Meanwhile, we also see that the performance of SAM2 does not significantly drop from Task I to Task III, as the number of the classes increases. However, this phenomenon does not apply to other baseline models. Lastly, another observation is that the sampling rate of this dataset is relatively low, yielding noncontinuous image sequences, making it even more challenging for SAM2 to segment and track.

TABLE IV: Quantitative Evaluation of Instrument Segmentation on EndoNeRF Dataset (Numbers in %).

Method	re-initialization	EndoNeRF-Cutting			EndoNeRF-Pulling		
		mDice	mIoU	mMae	mDice	mIoU	mMae
SAM2-Points-Center	-	97.32	94.80	0.78	90.43	84.02	0.99
SAM2-Points-Center	60 frames	97.97	96.02	0.59	90.43	84.02	1.00
SAM2-Points-Center	30 frames	98.10	96.29	0.55	90.51	84.12	0.99
SAM2-Points-Center	10 frames	98.15	96.37	0.54	89.01	82.30	1.06
SAM2-Points-Center	5 frames	98.17	96.40	0.54	90.46	84.11	0.99
SAM2-Points-Random 1	-	97.39	94.91	0.76	90.26	83.74	1.02
SAM2-Points-Random 1	60 frames	97.96	96.00	0.59	90.38	83.89	1.02
SAM2-Points-Random 1	30 frames	80.57	78.48	3.03	90.42	83.98	1.01
SAM2-Points-Random 1	10 frames	92.02	89.98	1.38	88.94	82.20	1.07
SAM2-Points-Random 1	5 frames	88.62	86.71	2.03	82.46	75.91	1.83
SAM2-Points-Random 3	-	98.41	96.87	0.48	90.56	84.13	1.02
SAM2-Points-Random 3	60 frames	98.42	96.89	0.47	88.98	82.15	1.12
SAM2-Points-Random 3	30 frames	80.80	78.88	3.37	89.13	82.33	1.12
SAM2-Points-Random 3	10 frames	98.42	96.89	0.47	86.30	78.64	1.37
SAM2-Points-Random 3	5 frames	95.37	93.61	0.98	88.61	81.43	1.21
SAM2-Points-Random 5	-	98.19	96.45	0.54	90.27	83.72	1.04
SAM2-Bbox (Standard)	-	98.26	96.58	0.52	90.41	83.98	1.00
SAM2-Bbox	60 frames	98.27	96.60	0.52	90.41	83.98	1.00
SAM2-Bbox	30 frames	98.24	96.55	0.52	90.48	84.08	1.00
SAM2-Bbox	10 frames	98.24	96.54	0.52	89.56	82.98	1.05
SAM2-Bbox	5 frames	98.23	96.52	0.53	92.08	85.97	0.97
SAM2-Mask (Standard)	-	98.40	96.86	0.48	79.08	72.77	1.91
SAM2-Mask	60 frames	98.63	97.31	0.41	79.21	73.01	1.88
SAM2-Mask	30 frames	98.68	97.39	0.39	79.84	74.13	1.76
SAM2-Mask	10 frames	98.87	97.76	0.34	90.99	86.21	0.72
SAM2-Mask	5 frames	98.97	97.97	0.31	96.09	92.87	0.46

TABLE V: Ablation Study of Noise Perturbations for Prompts on EndoNeRF Dataset (Numbers in %).

Method	Noised	EndoNeRF-Cutting			EndoNeRF-Pulling		
		mDice	mIoU	mMae	mDice	mIoU	mMae
SAM2-Bbox (Standard)	-	98.26	96.58	0.52	90.41	83.98	1.00
SAM2-Bbox	0.1 scale	98.29	96.63	0.51	69.43	62.40	2.77
SAM2-Bbox	0.3 scale	94.52	91.63	1.17	56.66	45.04	5.44
SAM2-Bbox	0.5 scale	50.01	34.08	10.10	39.26	33.55	6.81
SAM2-Bbox	0.05 shift	97.58	95.29	0.70	65.35	58.09	3.02
SAM2-Bbox	0.1 shift	94.81	90.14	1.48	51.97	48.32	3.19
SAM2-Bbox	0.2 shift	15.80	8.61	13.98	18.08	13.37	11.46
SAM2-Bbox	0.1 scale + 0.05shift	94.99	90.47	1.43	65.81	58.96	2.91
SAM2-Bbox	0.3 scale + 0.1shift	92.78	86.88	1.95	52.01	48.31	3.20
SAM2-Bbox	0.5 scale + 0.2shift	66.86	50.46	7.53	41.17	36.13	9.67
SAM2-Mask (Standard)	-	98.40	96.86	0.48	79.08	72.77	1.91
SAM2-Mask	0.05 noise	89.32	80.84	3.17	85.35	77.76	1.50
SAM2-Mask	0.1 noise	76.35	62.30	8.23	87.12	79.48	1.34
SAM2-Mask	0.2 noise	66.91	52.56	9.18	34.81	29.12	8.13

F. Segmentation in Unlabelled Surgery Videos

This section evaluates SAM2 for surgical tool and tissue segmentation in unlabelled videos using three datasets: Cholec80, SurgToolLoc and SurgicalLive24. For those datasets with no ground truth, we typically start by automatically generating a mask for the first frame by SAM2 automatic mask generator to identify the object we need to track. This mask and the first frame then will be used to initialize the SAM2 video predictor.

Cholec80: Experiments on Cholec80 are performed with both

point prompts and mask prompts separately, where points and mask are both generated by SAM2 automatic mask generator.

The automatically generated mask initialization are effective for 80% of the videos. Successful cases were characterized by clear initial frames containing surgical tools, enabling high-quality mask generation and subsequent accurate tracking (Figure 12).

SurgToolLoc: The first column of Figure 10 depicts an representative example of the automatically generated mask of the first frame on SurgToolLoc dataset. The points generated along

TABLE VI: Quantitative evaluation on CholecSeg8k Dataset with different prompts.

Method	Reinitialization	Mean IoU	Mean Dice	Tissues IoU	Instruments IoU	Tissues Dice	Instruments Dice
Mask2Former[15]	-	69.10%	-	-	-	-	-
HRNet32[15]	-	61.10%	-	-	-	-	-
HRNet32 + SP-TCN[15]	-	65.37%	-	-	-	-	-
Swin base[15]	-	68.42%	-	-	-	-	-
Swin base + SP-TCN[15]	-	69.38%	-	-	-	-	-
SAM2-Points-Random 1 (Standard)	-	63.43%	71.53%	55.47%	69.86%	70.18%	76.40%
SAM2-Points-Random 1	60 frames	65.09%	73.32%	57.28%	72.22%	71.34%	79.29%
SAM2-Points-Random 1	30 frames	64.72%	73.06%	56.83%	70.81%	71.32%	77.70%
SAM2-Points-Random 1	10 frames	65.90%	74.28%	58.02%	75.13%	72.08%	82.23%
SAM2-Points-Random 1	5 frames	65.77%	74.18%	57.64%	75.72%	71.75%	82.83%
SAM2-Points-Random 3 (Standard)	-	71.24%	79.17%	63.76%	77.64%	77.14%	84.06%
SAM2-Points-Random 3	60 frames	71.64%	79.50%	64.03%	79.29%	77.37%	85.76%
SAM2-Points-Random 3	30 frames	72.58%	80.39%	65.46%	78.99%	78.43%	85.59%
SAM2-Points-Random 3	10 frames	73.48%	81.30%	66.25%	81.63%	79.09%	88.23%
SAM2-Points-Random 3	5 frames	73.34%	81.23%	66.15%	82.01%	77.14%	84.06%
SAM2-Points-Center (Standard)	-	61.98%	70.08%	60.72%	76.00%	67.20%	82.97%
SAM2-Points-Center	60 frames	62.08%	70.20%	60.73%	77.03%	67.15%	83.93%
SAM2-Points-Center	30 frames	62.38%	70.40%	60.97%	78.12%	67.26%	84.85%
SAM2-Points-Center	10 frames	62.68%	70.80%	61.21%	79.60%	67.50%	86.29%
SAM2-Points-Center	5 frames	62.65%	70.84%	61.38%	80.21%	67.44%	86.98%
SAM2-Points-Center (1 negative point)	-	62.62%	70.75%	61.93%	75.69%	68.16%	82.81%
SAM2-Points-Center (3 negative points)	-	61.54%	69.88%	61.64%	73.52%	67.57%	80.20%
SAM2-Bbox (Standard)	-	83.34%	89.00%	82.15%	79.98%	89.13%	85.85%
SAM2-Bbox	60 frames	84.31%	89.89%	83.07%	81.66%	89.92%	87.58%
SAM2-Bbox	30 frames	84.93%	90.49%	83.71%	83.12%	90.35%	89.04%
SAM2-Bbox	10 frames	86.11%	91.57%	84.88%	84.83%	91.34%	90.74%
SAM2-Bbox	5 frames	86.50%	91.90%	85.32%	85.57%	91.63%	91.49%
SAM2-Mask (Standard)	-	88.95%	92.73%	88.40%	81.62%	93.49%	86.83%
SAM2-Mask	60 frames	90.14%	93.69%	89.64%	84.04%	94.27%	89.05%
SAM2-Mask	30 frames	91.14%	94.48%	90.59%	86.24%	94.86%	90.95%
SAM2-Mask	10 frames	92.85%	95.77%	92.40%	89.19%	95.98%	93.35%
SAM2-Mask	5 frames	93.93%	96.48%	93.55%	91.04%	96.60%	91.49%

with mask by automatic mask generator are then used as the point prompts for SAM2 video predictor to generate masks in the subsequent frames of the video clip.

The qualitative segmentation performance of SAM 2 across time frames is demonstrated in Figure 10. The second to fifth column show the results of the frames at $t = 0, 10, 20, 30$ s, respectively. SAM 2 delivers reliable segmentation results for both surgical tools and tissue when the endoscopic scene is well-lit and the surgical tools exhibit smooth motion.

SurgicalLive24: The performance varies depending on the type of surgeries (Figure 11). In narrow surgical video scenarios, such as urethroscopy (Figure 11 (k)), the overall segmentation effect is not satisfactory. This may be due to the low resolution of the video itself and the blur caused by the rapid changes of objects in narrow scenes. In scenarios such as thoracoscopy and laparoscopy, which are well lit and relatively open, SAM2 can achieve good segmentation and tracking results for surgical instruments. For tissues and organs, it is difficult to track them over long video sequences, due to the unclear boundaries of organs and tissues. Changes in the scene, such as the movement of camera or the introduction of new organs and tissues, can hinder the tracking of tissues and organs.

G. Ablation Study

To evaluate the robustness and adaptability of our proposed SAM2 framework, we conducted an ablation study on the CholecSeg8k and Endovis17 datasets, focusing on the impact of noise and, for CholecSeg8k, the effectiveness of new object detection.

Robustness to Noise: We investigated the impact of introducing noise into the initial prompts, specifically focusing on scale and shift variations.

- Scale noise was applied as a scaling factor, where 1.0 denotes "no change" and 0.5 represents a zoom-out to 50 percent of the original size.
- Shift noise was applied as a translation fraction of the image height/width, represented as (x -translation, y -translation), where 0 denotes "no change" and 0.5 denotes "half of the axis size."

For mask prompts, in addition to the combination of scale and shift noise, we also introduce erosion and dilation.

Table IX presents the results of applying different levels of noise to both bounding box and mask prompts on the CholecSeg8k dataset. The results demonstrate that SAM2's performance is highly sensitive to the quality of the initial prompts. As the level of noise increases, both the mean Intersection over Union (IoU) and Dice scores decrease significantly. For instance, in the case of bounding box prompting, adding a 0.5 shift in the prompt reduces the IoU from 0.8334

TABLE VII: Quantitative evaluation on Endoscopes-Seg50 dataset (Numbers in %)

Method	Reinitialization	mIoU	mDice	Tissue IoU	Tool IoU	Tissue Dice	Tool Dice
DLV3P-R50-SurgMoCov2 [5]	-	15.07	24.83	-	-	-	-
DLV3P-R50-SurgDINO [5]	-	16.94	26.51	-	-	-	-
DLV3P-R50 [5]	-	14.65	22.62	-	-	-	-
DLV3P-R50-SurgMoCov2 [5]	-	15.70	24.05	-	-	-	-
DLV3P-R50-SurgDINO [5]	-	14.05	21.79	-	-	-	-
SelfPromptSAM [35]	-	2.6	3.53	-	-	-	-
SurgicalSAM [36]	-	6.90	10.50	-	-	-	-
PerSAM [40]	-	4.42	7.97	-	-	-	-
PerSAM-F [40]	-	4.61	8.33	-	-	-	-
PerSAM-F-MedSAM [40], [22]	-	3.38	6.81	-	-	-	-
CycleSAM-VIT [25]	-	8.17	14.26	-	-	-	-
CycleSAM-SurgDINO [25]	-	15.52	22.13	-	-	-	-
CycleSAM-SurgMoCov2 [25]	-	16.40	24.05	-	-	-	-
CycleSAM-DLV3P-SurgDINO [25]	-	20.56	28.48	-	-	-	-
CycleSAM-DLV3P-SurgMoCov2 [25]	-	22.34	30.86	-	-	-	-
DLV3P-R50-FullSup [5]	-	45.02	57.60	-	-	-	-
SAM2-Points-Random 1	-	20.76	25.95	13.35	57.48	17.96	65.77
SAM2-Points-Random 1	60 frames	23.64	29.60	16.48	61.67	22.27	69.62
SAM2-Points-Random 1	30 frames	36.38	44.43	28.99	75.69	36.59	83.50
SAM2-Points-Random 3	-	27.16	33.37	19.15	59.38	24.69	67.58
SAM2-Points-Random 3	60 frames	28.64	34.98	21.16	64.36	27.23	71.52
SAM2-Points-Random 3	30 frames	41.12	48.88	29.38	81.88	37.54	88.97
SAM2-Points-Center	-	20.79	26.07	13.64	56.59	18.29	64.96
SAM2-Points-Center	30 frames	37.98	45.64	29.55	80.17	37.21	87.80
SAM2-Points-Random 5	-	26.41	32.96	19.11	61.65	24.86	69.40
SAM2-Points-Random 1	3 neg	28.24	35.15	19.69	55.63	25.10	64.55
SAM2-Points-Random 1	1 neg	26.76	32.83	18.11	56.98	23.20	65.65
SAM2-Bbox (Standard)	-	38.94	44.88	34.34	61.92	39.86	69.96
SAM2-Bbox	60 frames	49.32	56.39	45.96	66.10	53.07	73.03
SAM2-Bbox	30 frames	76.82	85.87	75.00	85.96	84.62	92.15
SAM2-Mask (Standard)	-	47.82	51.81	42.67	73.62	46.14	80.15
SAM2-Mask	60 frames	63.79	66.54	60.42	80.65	62.90	84.76
SAM2-Mask	30 frames	98.91	99.45	98.85	99.18	99.42	99.59

to 0.4544 and the Dice score from 0.8900 to 0.5128. Similarly, for mask prompting, a 0.5 noise level results in an IoU drop from 0.8895 to 0.4836 and a Dice score decrease from 0.9273 to 0.5523. Figure 13 visually illustrates the degradation in segmentation quality caused by noisy prompts. This sensitivity highlights the importance of accurate and precise prompts for achieving optimal performance with SAM2.

We further explored the impact of noise on the Endovis17 dataset, as summarized in Figure 14. Our findings suggest that SAM2 exhibits robustness to slight noise levels on this dataset. When applying shift, scale, and combined shift and scale noise to bounding box prompts, and composite noise to mask prompts at 0.1 intensity, the mIoU decreases by approximately 1%, 0%, 7%, and 3%, respectively. Notably, scale noise appears to have less influence than shift noise for bounding box prompts, indicating greater robustness in handling scale variations. While significant noise levels can hinder the tracking of surgical instruments in some videos, the majority of videos in Endovis17 remain segmentable with reasonable clarity.

Effectiveness of New Object Detection on CholecSeg8k:

We explored the benefits of incorporating new object detection prompts into the SAM2 pipeline on the CholecSeg8k dataset. Table X summarizes the results for various prompting methods. In general, introducing new object detection prompts leads

to improved segmentation accuracy across all methods. For example, point prompting with a center point shows a slight increase in performance, with the IoU rising from 0.6198 to 0.6255 and the Dice score from 0.7008 to 0.7071. Bounding box prompting also benefits from new object detection, as evidenced by the IoU increase from 0.8334 to 0.8459 and the Dice score improvement from 0.8900 to 0.9034. Mask prompting exhibits the most significant improvement, with the IoU increasing from 0.8895 to 0.9036 and the Dice score rising from 0.9273 to 0.9415. These results suggest that new object detection aids SAM2 in adapting to changes in the scene and improving segmentation accuracy. However, it’s worth noting that the performance with new object detection is still not as good as reinitialization with an interval of 10 or 5 frames, which suggests that further refinements to the new object detection mechanism could yield even greater improvements.

VI. FAILURE CASE ANALYSIS

The SAM2 model, when applied to various surgical datasets, encountered several challenges that impacted its performance in surgical tool tracking and segmentation tasks. These challenges primarily fell into two categories: (1) failure cases in datasets with ground truth annotations, and (2) issues arising from AutoMask generation and its application as pseudo labels in datasets lacking ground truth. In the first category, key

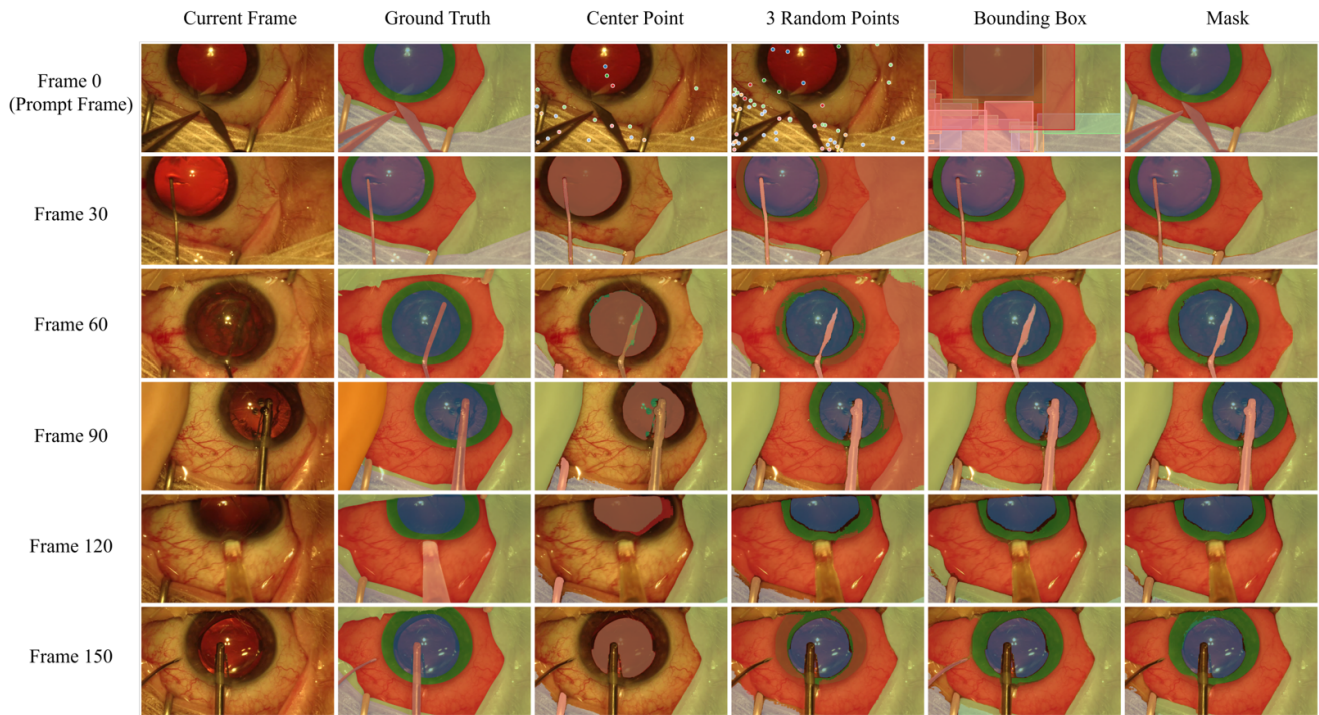


Fig. 9: Visualization of segmentation results on the CaDISv2 dataset

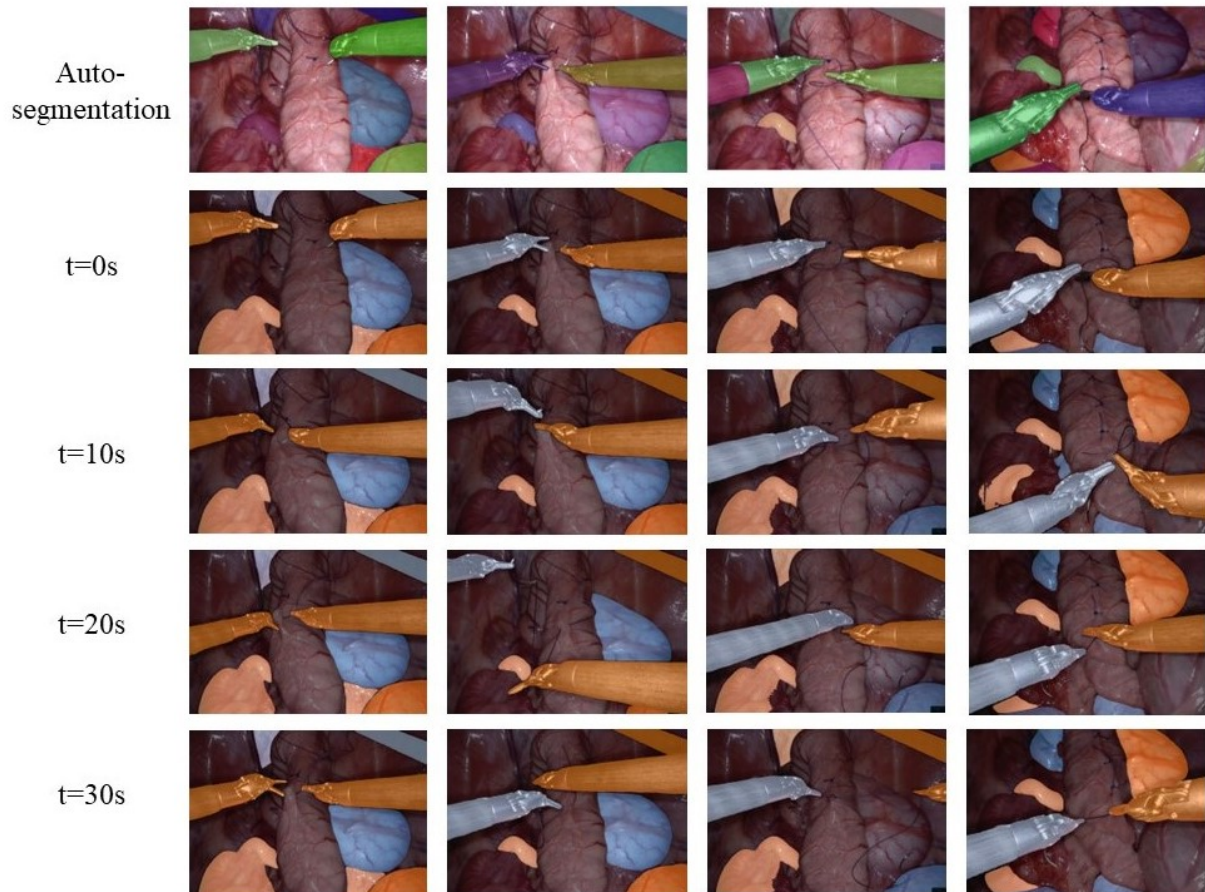


Fig. 10: Visualization of segmentation results on the SurgToolLoc dataset

TABLE VIII: Quantitative evaluation on CaDIS dataset (Numbers in %)

Method	Reinitialize Frames	Task I (8 classes)			Task II (17 classes)			Task III (25 classes)		
		mIoU (%)	PA (%)	PAC (%)	mIoU (%)	PA (%)	PAC (%)	mIoU (%)	PA (%)	PAC (%)
UNet	-	83.3	94.4	88.9	70.2	94.3	80.2	59.3	94.1	71.6
DeepLabv3+	-	85.6	94.8	91.5	75.8	94.7	84.9	65.9	94.7	78.1
UPerNet	-	85.9	94.7	91.7	77.0	94.7	84.9	70.1	94.4	80.4
HRNetV2	-	85.5	94.5	91.6	76.3	94.5	85.1	68.0	94.5	78.6
OCRNet	-	85.5	94.8	90.9	76.3	94.5	85.4	70.2	94.6	80.8
PSPNet	-	85.1	94.6	84.2	75.6	94.6	84.2	66.1	94.4	77.5
SegFormer	-	85.4	94.5	91.4	77.7	94.4	86.3	70.2	94.4	81.1
SegNeXt	-	85.8	94.8	91.9	77.5	94.6	85.7	70.0	94.6	80.5
STswinCL	-	85.7	94.6	91.4	77.3	94.6	84.5	69.7	94.5	78.6
LSKANet	-	86.1	94.9	91.8	77.9	94.7	85.7	71.1	94.6	81.2
SAM2-Points-Center	-	35.5	83.8	45.9	30.2	84.1	39.3	30.2	84.1	39.3
SAM2-Points-Center	60 frames	37.8	84.6	49.9	33.2	84.6	44.5	32.1	84.4	43.2
SAM2-Points-Center	30 frames	40.9	85.1	53.5	35.8	85.2	47.5	35.6	85.0	47.3
SAM2-Points-Center	15 frames	43.4	84.5	56.9	40.1	84.7	53.0	40.5	84.6	53.6
SAM2-Points-Center	10 frames	44.6	84.7	58.0	42.3	84.8	55.3	42.3	84.8	55.4
SAM2-Points-Random 1	-	49.6	89.2	64.1	43.9	88.1	58.9	43.6	88.6	58.0
SAM2-Points-Random 1	60 frames	49.1	89.1	64.9	45.2	89.5	59.2	43.3	88.0	58.7
SAM2-Points-Random 1	30 frames	50.0	88.4	67.3	45.8	88.9	61.7	45.4	88.6	61.1
SAM2-Points-Random 1	15 frames	52.7	88.8	69.8	50.1	88.6	66.9	49.7	88.4	67.0
SAM2-Points-Random 1	10 frames	54.0	88.7	71.8	52.1	89.3	69.2	51.9	88.8	69.2
SAM2-Points-Random 3	-	53.0	88.9	69.3	47.0	89.4	62.0	47.3	89.2	62.0
SAM2-Points-Random 3	60 frames	53.5	89.5	71.2	48.2	89.6	64.8	47.3	89.6	63.6
SAM2-Points-Random 3	30 frames	56.5	90.4	73.7	49.7	89.7	66.5	49.1	89.3	66.5
SAM2-Points-Random 3	15 frames	58.7	90.1	77.5	54.8	90.0	73.1	54.9	89.8	73.4
SAM2-Points-Random 3	10 frames	59.5	89.7	78.9	56.8	89.6	75.8	57.0	89.8	75.9
SAM2-Points-Random 5	-	55.3	91.7	68.9	48.6	91.1	62.1	49.3	91.3	62.5
SAM2-Points-3 neg	-	35.8	84.3	46.5	29.6	85.7	38.3	30.9	85.5	39.2
SAM2-Points-1 neg	-	36.3	84.6	46.0	30.6	85.0	38.5	30.7	85.3	38.8
SAM2-Bbox (Standard)	-	56.8	94.9	66.3	50.8	94.9	59.3	50.8	94.9	59.3
SAM2-Bbox	60 frames	58.4	94.9	68.5	53.2	94.9	62.5	52.0	94.9	61.1
SAM2-Bbox	30 frames	61.1	95.0	71.6	55.2	95.0	64.7	54.9	94.9	64.4
SAM2-Bbox	15 frames	64.7	95.1	75.6	60.4	95.1	70.8	60.6	95.1	71.1
SAM2-Bbox	10 frames	66.4	95.1	77.2	63.4	95.2	74.0	63.4	95.1	74.0
SAM2-Mask (Standard)	-	64.6	97.7	69.8	58.3	97.7	62.6	58.3	97.7	62.6
SAM2-Mask	60 frames	67.2	97.9	72.0	61.8	97.9	65.9	60.6	97.8	64.5
SAM2-Mask	30 frames	70.7	98.2	75.4	64.5	98.1	68.3	64.3	98.1	68.1
SAM2-Mask	15 frames	75.1	98.4	79.7	70.7	98.4	74.8	70.9	98.4	75.1
SAM2-Mask	10 frames	77.0	98.5	81.3	73.8	98.6	77.9	73.9	98.5	78.0

issues included difficulties with prompting and initialization, instrument identification and confusion, and maintaining temporal consistency. The second category revealed challenges in generating accurate initial segmentations and propagating them to subsequent frames. This analysis explores these failure cases in detail, providing insights into areas for improvement and future research directions.

In datasets with ground truth annotations, the SAM2 model encountered several significant challenges, primarily related to prompting and initialization. The quality and placement of initial prompts proved crucial in guiding accurate segmentation. This was particularly evident in various scenarios encountered during the model’s application. Multi-part objects presented unique challenges in prompting, especially in the CholecSeg8k dataset. When dealing with large multi-part objects in single-point prompting, incorrect prompt placements often occur due to overlapping object centers (Figure 15-(a)). This highlighted the complexity of accurately identifying and segmenting objects with multiple components. Bounding box prompting faced difficulties with complex and irregularly

shaped objects. In the EndoVis18 dataset, for instance, closely connected objects with overlapping boxes posed significant challenges in bounding box prompt experiments (Figure 15-(b) and (c)). This underscored the limitations of bounding box approaches when dealing with intricate object geometries and spatial relationships. Incomplete object appearance in prompt frames, such as when only a tool’s tip was visible, significantly affected segmentation in subsequent frames (Figure 15-(d)). This scenario highlighted the model’s sensitivity to partial object visibility during the prompting phase, emphasizing the need for robust handling of incomplete visual information.

The model also struggled with instrument identification and confusion, particularly when dealing with similar instruments in dynamic scenarios. In the EndoVis17 dataset, the model occasionally confused new instruments appearing in locations similar to previously prompted ones. This issue was particularly evident when an instrument was removed from the frame and then reintroduced, indicating a need for better long-term memory or context understanding. Instrument blurriness further contributed to identification problems, making it chal-

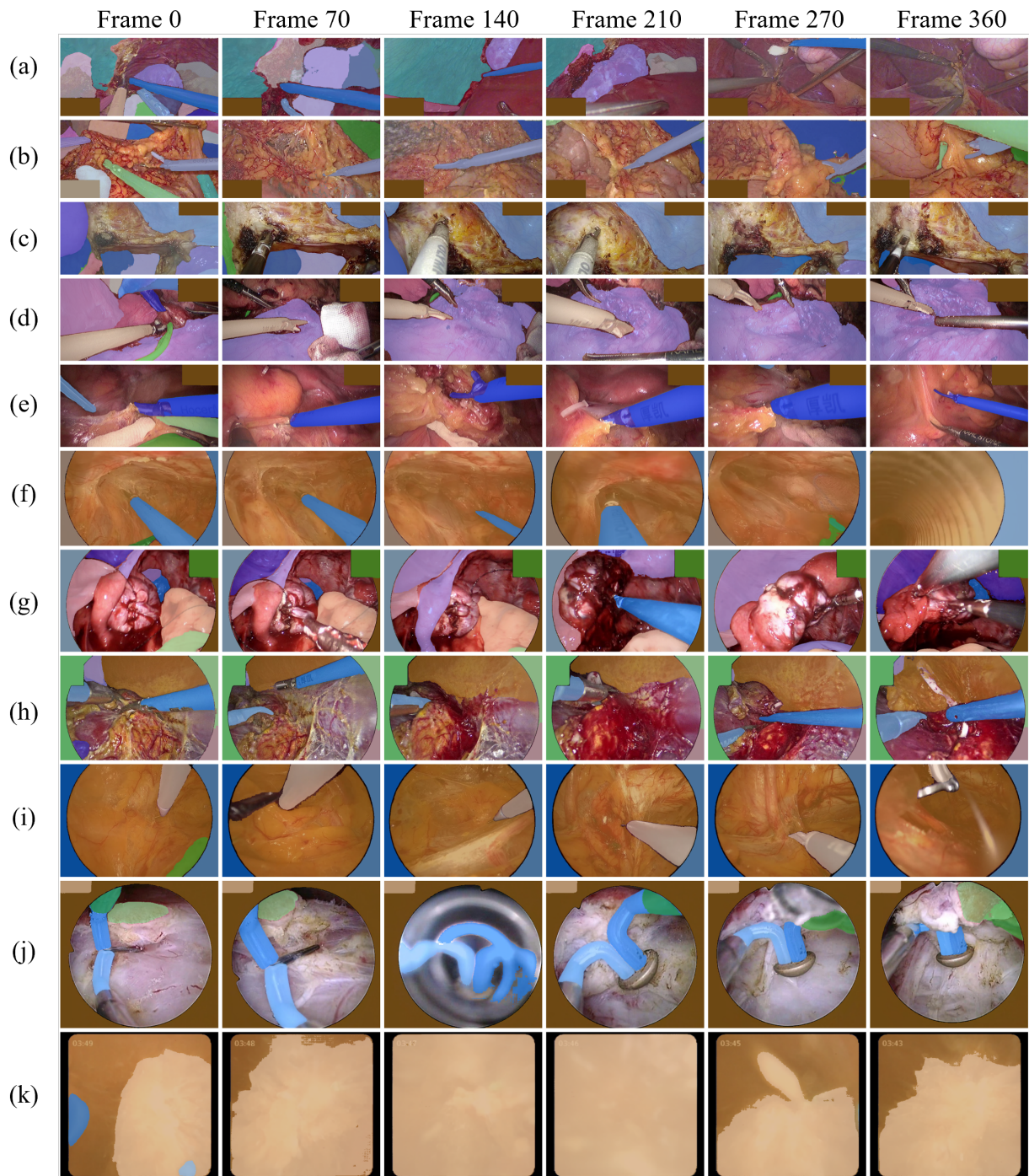


Fig. 11: Results on SurgicalLive24 Dataset with various types of surgical videos. Rows correspond to the following procedures: (a) Laparoscopic pancreatic tumor resection with fluorescence guidance (b) Laparoscopic gastrectomy for gastric cancer with fluorescence guidance (c) Total laparoscopic hysterectomy via single-port (d) Laparoscopic radical antegrade modular pancreateosplenectomy (L-RAMPS) (e) Laparoscopically-assisted radical resection of sigmoid colon cancer (f) Thoracoscopically-assisted resection of right anterior mediastinal tumor (g) Laparoscopic ovarian cystectomy (h) Laparoscopic right adrenalectomy (i) Bilateral inguinal hernia repair via Totally Extraperitoneal (TEP) approach (j) Transurethral resection of bladder tumor (TURBT) (k) Ureteroscopy with laser lithotripsy and stone extraction

lensing for SAM2 to accurately distinguish between different instruments.

For datasets lacking ground truth annotations, such as SurgToolLoc and Cholec80, an AutoMask generation approach

was employed for the first frame as a pseudo label. This introduced a second category of challenges related to the accuracy of the initial segmentation and its propagation to subsequent frames. In cases where the initial frame was clear

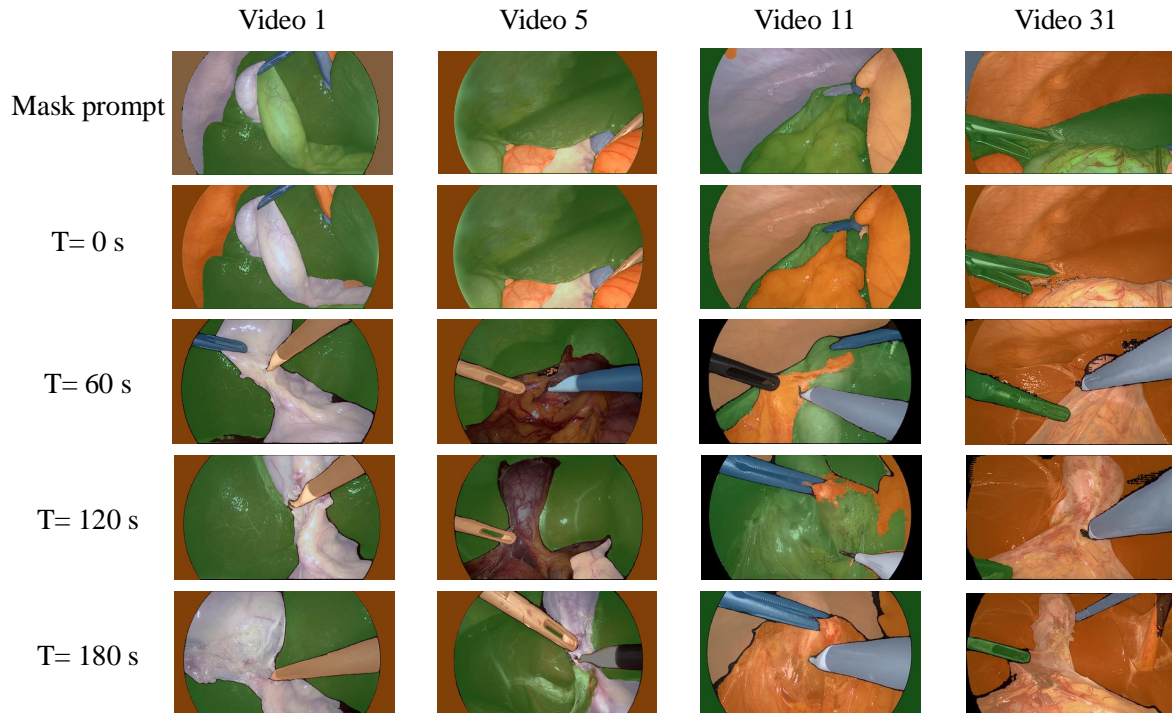


Fig. 12: Representative Frames in Cholec80

TABLE IX: CholecSeg8k - Ablation Study on Noise Perturbation

Method	Noised	Mean IoU	Mean Dice	Tissues IoU	Instruments IoU	Tissues Dice	Instruments Dice
SAM2-Bbox (Standard)	-	83.34%	89.00%	82.15%	79.98%	89.13%	85.85%
SAM2-Bbox	0.1 scale	80.01%	86.29%	79.69%	79.00%	86.48%	85.16%
SAM2-Bbox	0.3 scale	70.24%	77.52%	70.60%	69.46%	78.70%	75.81%
SAM2-Bbox	0.5 scale	61.69%	69.28%	60.18%	62.16%	68.56%	68.30%
SAM2-Bbox	0.1 shift	67.18%	74.88%	66.84%	62.95%	75.10%	69.84%
SAM2-Bbox	0.3 shift	47.86%	54.41%	47.97%	43.81%	54.76%	47.88%
SAM2-Bbox	0.5 shift	45.44%	51.28%	44.98%	37.47%	51.15%	40.94%
SAM2-Bbox	0.1 shift+scale	65.82%	73.33%	65.48%	63.54%	73.42%	70.38%
SAM2-Bbox	0.3 shift+scale	47.34%	53.96%	45.92%	39.74%	52.97%	43.86%
SAM2-Bbox	0.5 shift+scale	46.59%	52.87%	44.48%	41.33%	51.05%	45.30%
SAM2-Mask (Standard)	-	88.95%	92.73%	88.40%	81.62%	93.49%	86.83%
SAM2-Mask	0.1 noise	68.37%	76.30%	67.44%	55.22%	75.84%	62.49%
SAM2-Mask	0.3 noise	55.01%	62.84%	53.43%	53.98%	61.53%	59.63%
SAM2-Mask	0.5 noise	48.36%	55.23%	48.55%	41.47%	55.45%	46.48%

and contained surgical tools, both point and mask prompts performed well in generating initial segmentations. However, when the initial frame was blurry or lacked surgical tools, a later frame had to be selected for initialization, potentially introducing inconsistencies in the tracking process.

Segmentation boundary issues manifested in various forms in the SurgToolLoc dataset when applying AutoMask-generated pseudo labels. Over-segmentation of tissues resulted in large regions being divided into multiple irregular small areas, indicating issues with spatial continuity (Figure 16-(a)). Additionally, erroneous merging occurred as shown in Figure 16-(b), where surgical instruments were sometimes segmented together with each other, blurring the boundaries between distinct elements. Incorrect boundary delineation was another

notable issue, with single instruments sometimes incorrectly divided or unidentified after exiting and re-entering the frame, as illustrated in Figure 16-(c)). The Cholec80 dataset revealed additional challenges in the AutoMask approach, as the SAM2 model struggled with segmenting different parts of internal organs effectively. This stemmed from its inability to distinguish different parts of internal organs in the initial frame used for mask generation, leading to inconsistent segmentations in subsequent frames (Figure 16-(d)).

To address these challenges and improve the SAM2 model's performance in surgical applications, future research should focus on several key areas. For datasets with ground truth, enhancing the model's ability to handle complex prompting scenarios, improving instrument identification for similar tools,

TABLE X: CholecSeg8k - Ablation New Object Prompt Initialization

Method	New Object Initialization	Mean IoU	Mean Dice	Tissues IoU	Instruments IoU	Tissues Dice	Instruments Dice
SAM2-Points-Random 1 (Standard)	-	63.43%	71.53%	55.47%	69.86%	70.18%	76.40%
SAM2-Points-Random 1	Yes	65.44%	73.97%	57.61%	73.72%	71.88%	80.81%
SAM2-Points-Random 3 (Standard)	-	71.24%	79.17%	63.76%	77.64%	77.14%	84.06%
SAM2-Points-Random 3	Yes	72.72%	80.67%	65.75%	78.92%	78.63%	85.49%
SAM2-Points-Center (Standard)	-	61.98%	70.08%	60.72%	76.00%	67.20%	82.97%
SAM2-Points-Center	Yes	62.55%	70.71%	61.26%	78.04%	67.44%	85.18%
SAM2-Bbox (Standard)	-	83.34%	89.00%	82.15%	79.98%	89.13%	85.85%
SAM2-Bbox	Yes	84.59%	90.34%	83.12%	83.35%	90.00%	89.52%
SAM2-Mask (Standard)	-	88.95%	92.73%	88.40%	81.62%	93.49%	86.83%
SAM2-Mask	Yes	90.36%	94.15%	89.59%	85.40%	94.43%	90.78%

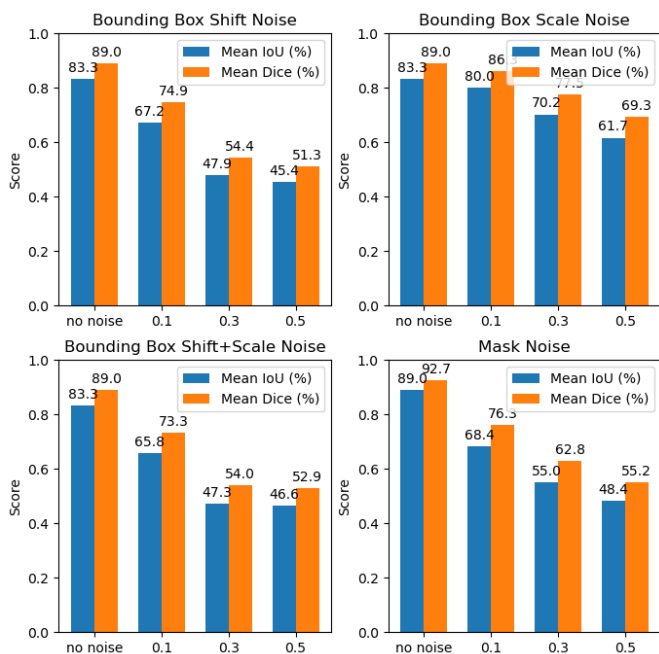


Fig. 13: Ablation Study on Noise Perturbation on CholecSeg8k Dataset.

and developing better strategies for maintaining temporal consistency is crucial. For datasets requiring AutoMask generation, refining the initial segmentation process, improving the model's ability to propagate segmentations accurately across frames, and developing more robust techniques for handling varying image qualities and content are essential. By addressing these challenges, the utility of the SAM2 model in real-world surgical applications can be significantly advanced, potentially leading to more accurate and reliable tool tracking and segmentation in diverse surgical scenarios.

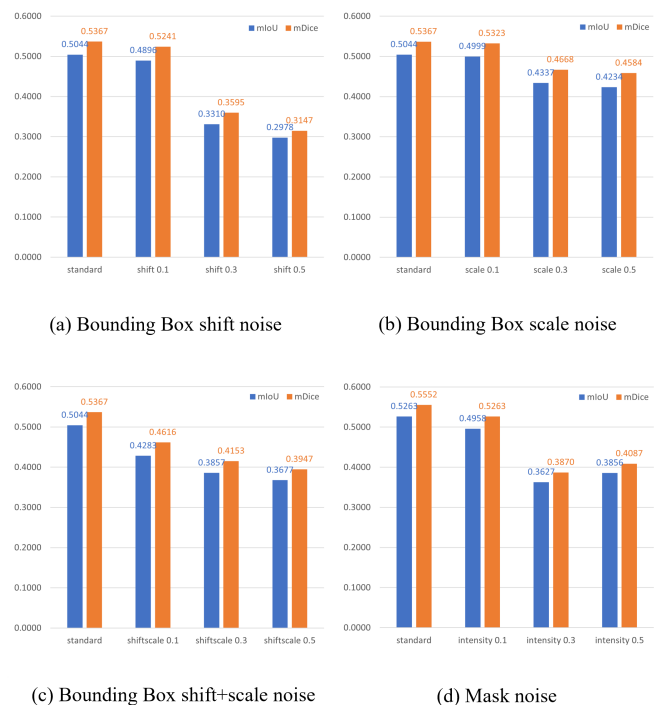


Fig. 14: Ablation Study on Noise Perturbation on Endovis17 Dataset.

REFERENCES

- [1] Britty Baby, Daksh Thapar, Mustafa Chasmai, Tamajit Banerjee, Kunal Dargan, Ashish Suri, Subhashis Banerjee, and Chetan Arora. From forks to forceps: A new framework for instance segmentation of surgical instruments. In *Proceedings of the IEEE/CVF winter conference on applications of computer vision*, pages 6191–6201, 2023. II
- [2] Deepak Baby et al. S3net: Surgical scene segmentation network for endoscopic vision. *Medical Image Analysis*, 82:102638, 2023. III
- [3] Yutong Ban, Jennifer A Eckhoff, Thomas M Ward, Daniel A Hashimoto, Ozanan R Meireles, Daniela Rus, and Guy Rosman. Concept graph neural networks for surgical video understanding. *IEEE Transactions on Medical Imaging*, 2023. II-A
- [4] Yutong Ban, Guy Rosman, Jennifer A Eckhoff, Thomas M Ward, Daniel A Hashimoto, Taisei Kondo, Hidekazu Iwaki, Ozanan R Meireles, and Daniela Rus. Supr-gan: surgical prediction gan for event anticipation in laparoscopic and robotic surgery. *IEEE Robotics and Automation Letters*, 7(2):5741–5748, 2022. II-A
- [5] Liang-Chieh Chen, Yukun Zhu, George Papandreou, Florian Schroff, and Hartwig Adam. Encoder-decoder with atrous separable convolution

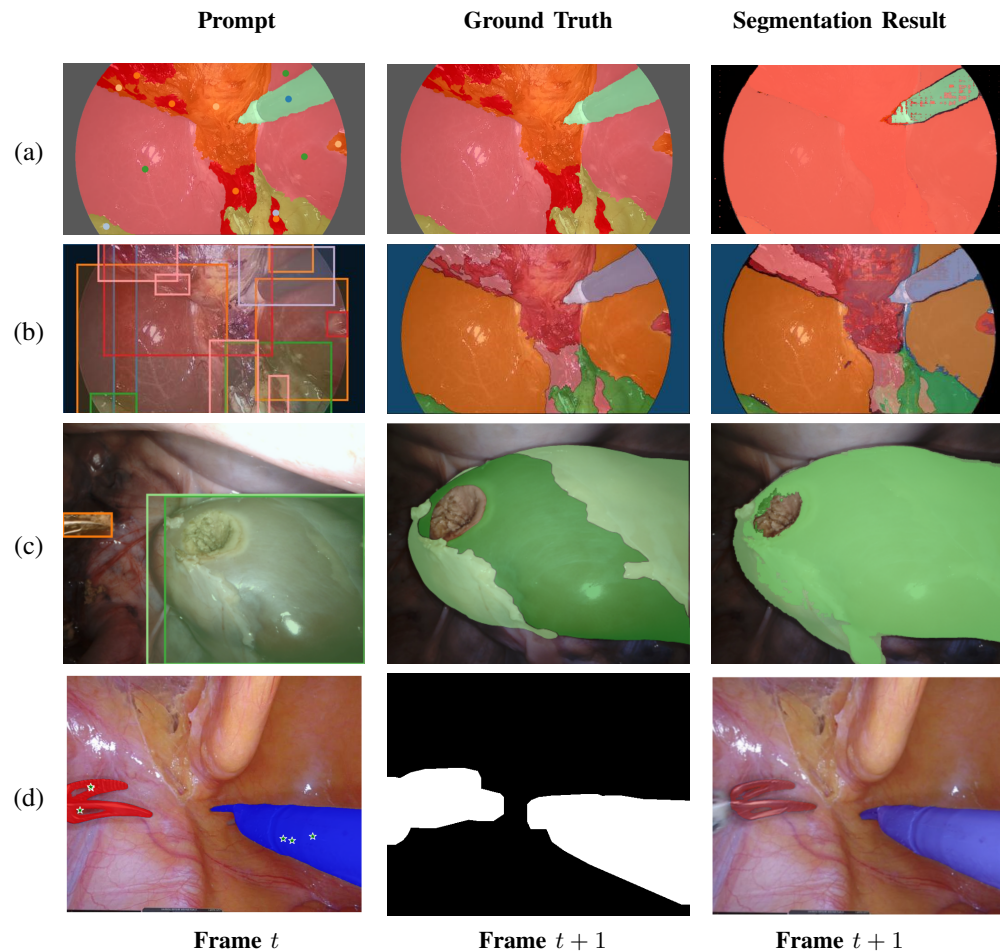


Fig. 15: Failure cases analysis in datasets with ground truth annotations. Common failure cases due to (a) Single-point prompting for multi-part objects (CholecSeg8k). (b) Bounding box prompting for complex objects (CholecSeg8k). (c) overlapping bounding box prompts (EndoVis18). (d) Incomplete object appearance prompt (EndoNerf).

- for semantic image segmentation. In *Proceedings of the European conference on computer vision (ECCV)*, pages 801–818, 2018. VII
- [6] Bowen Cheng, Alexander G Schwing, and Alexander Kirillov. Mask2former: Masked transformer for end-to-end instance segmentation. In *Proceedings of the IEEE/CVF Conference on Computer Vision and Pattern Recognition*, pages 14819–14828, 2021. III
- [7] Tianfei Cheng, Xialei Wang, Ling Chen, and Qixiang Zhang. Boundary-preserving mask r-cnn. In *European Conference on Computer Vision*, pages 660–676. Springer, 2020. III
- [8] Magdalena K Chmarra, CA Grimbergen, and J Dankelman. Systems for tracking minimally invasive surgical instruments. *Minimally Invasive Therapy & Allied Technologies*, 16(6):328–340, 2007. II-B
- [9] Emanuele Colleoni and Danaïl Stoyanov. Robotic instrument segmentation with image-to-image translation. *IEEE Robotics and Automation Letters*, 6(2):935–942, 2021. II-B
- [10] Rohan Raju Dhanakshirur, KN Ajay Shastry, Kaustubh Borgavi, Ashish Suri, Prem Kumar Kalra, and Chetan Arora. Learnable query initialization for surgical instrument instance segmentation. In *International Conference on Medical Image Computing and Computer-Assisted Intervention*, pages 728–738. Springer, 2023. V-C, III
- [11] Xiaofei Du, Thomas Kurmann, Ping-Lin Chang, Maximilian Allan, Sebastien Ourselin, Raphael Sznitman, John D Kelly, and Danaïl Stoyanov. Articulated multi-instrument 2-d pose estimation using fully convolutional networks. *IEEE transactions on medical imaging*, 37(5):1276–1287, 2018. II-B
- [12] Haozhi Fang, Jian Sun, Jing Chen, Yichen Wang, Hang Zhao, and Zhanyi Yao. Queryinst: Parallel multiple instance queries for instance segmentation. In *Advances in Neural Information Processing Systems*, volume 34, pages 10837–10848, 2021. III
- [13] Robert Ganea and Sinisa Todorovic. Orienmask: Robust orientation estimation for instance segmentation. In *Proceedings of the IEEE/CVF Conference on Computer Vision and Pattern Recognition*, pages 2202–2211, 2021. III
- [14] Cristina González, Laura Bravo-Sánchez, and Pablo Arbelaez. Isinet: an instance-based approach for surgical instrument segmentation. In *International Conference on Medical Image Computing and Computer-Assisted Intervention*, pages 595–605. Springer, 2020. II, III
- [15] Maria Grammatikopoulou, Ricardo Sanchez-Matilla, Felix Bragman, David Owen, Lucy Culshaw, Karen Kerr, Danaïl Stoyanov, and Imanol Luengo. A spatio-temporal network for video semantic segmentation in surgical videos. *International Journal of Computer Assisted Radiology and Surgery*, 19(2):375–382, 2024. VI
- [16] Kaiming He, Xinlei Chen, Saining Xie, Yanghao Li, Piotr Dollár, and Ross Girshick. Masked autoencoders are scalable vision learners. In *Proceedings of the IEEE/CVF conference on computer vision and pattern recognition*, pages 16000–16009, 2022. III
- [17] Byeongho Heo, Song Park, Dongyoon Han, and Sangdoon Yun. Rotary position embedding for vision transformer. *arXiv preprint arXiv:2403.13298*, 2024. III
- [18] Vladimir Iglovikov and Alexey Shvets. Ternaunet: U-net with vgg11 encoder pre-trained on imagenet for image segmentation. *arXiv preprint arXiv:1801.05746*, 2018. II
- [19] Pierre Jannin, Mélanie Raimbault, Xavier Morandi, Laurent Riffaud, and Bernard Gibaud. Model of surgical procedures for multimodal image-guided neurosurgery. *Computer Aided Surgery*, 8(2):98–106, 2003. II-A
- [20] Yueming Jin, Keyun Cheng, Qi Dou, and Pheng-Ann Heng. Inco-

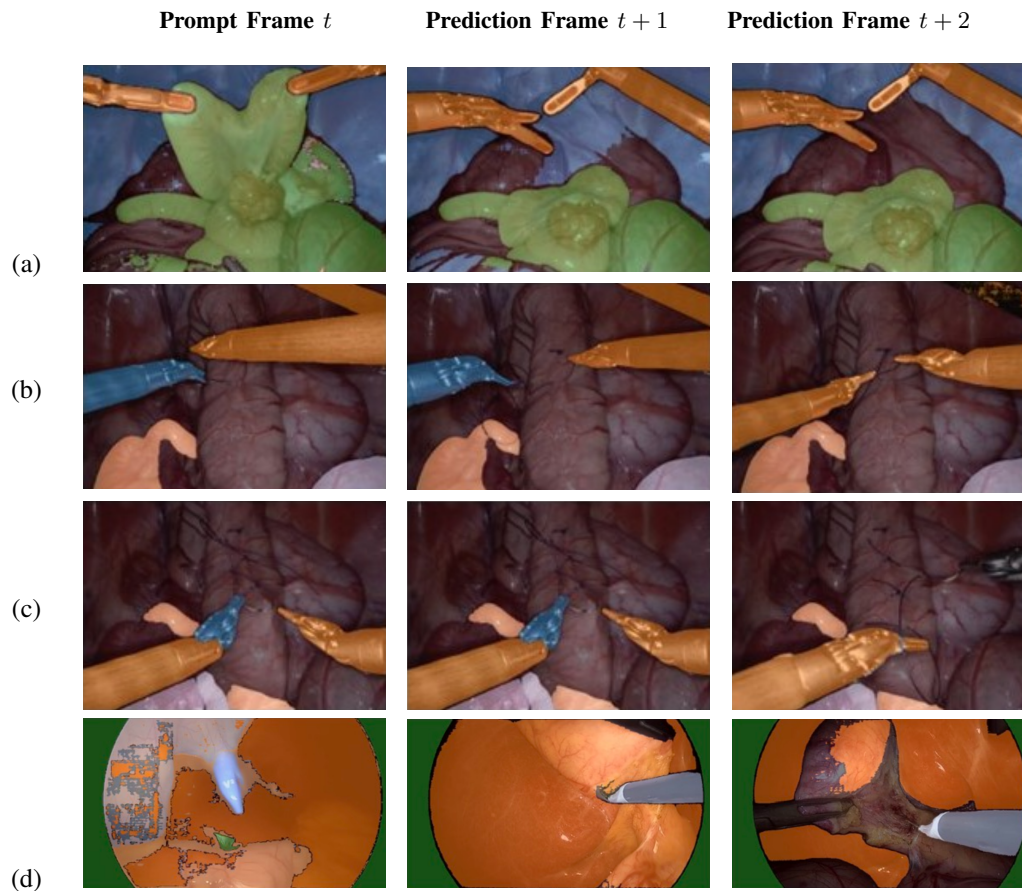


Fig. 16: Failure Cases Analysis for Unlabeled Surgical Videos. Common failure case due to (a) Over-segmentation of tissues using Auto-generated pseudo labels. (SurgToolLoc) (b) Erroneous merging of surgical instruments (SurgToolLoc). (c) Incorrect boundary delineation of AutoMask. (SurgToolLoc) (d) Difficulty in distinguishing different tissues (Cholec80)

- porating temporal prior from motion flow for instrument segmentation in minimally invasive surgery video. In *Medical Image Computing and Computer Assisted Intervention–MICCAI 2019: 22nd International Conference, Shenzhen, China, October 13–17, 2019, Proceedings, Part V 22*, pages 440–448. Springer, 2019. II
- [21] Alexander Kirillov, Eric Mintun, Nikhila Ravi, Hanzi Mao, Chloe Rolland, Laura Gustafson, Tete Xiao, Spencer Whitehead, Alexander C Berg, Wan-Yen Lo, et al. Segment anything. In *Proceedings of the IEEE/CVF International Conference on Computer Vision*, pages 4015–4026, 2023. III
- [22] Jun Ma, Yuting He, Feifei Li, Lin Han, Chenyu You, and Bo Wang. Segment anything in medical images. *Nature Communications*, 15(1):654, 2024. VII
- [23] L MacKenzie, JA Ibbotson, CGL Cao, and AJ Lomax. Hierarchical decomposition of laparoscopic surgery: a human factors approach to investigating the operating room environment. *Minimally Invasive Therapy & Allied Technologies*, 10(3):121–127, 2001. II-A
- [24] Tim Meinhardt, Alexander Kirillov, Laura Leal-Taixe, and Christoph Feichtenhofer. Trackformer: Multi-object tracking with transformers. In *Proceedings of the IEEE/CVF conference on computer vision and pattern recognition*, pages 8844–8854, 2022. II
- [25] Aditya Murali, Pietro Mascagni, Didier Mutter, and Nicolas Padoy. Cyclesam: One-shot surgical scene segmentation using cycle-consistent feature matching to prompt sam. *arXiv preprint arXiv:2407.06795*, 2024. VII
- [26] Chakka Sai Pradeep and Neelam Sinha. Spatio-temporal features based surgical phase classification using cnns. In *2021 43rd Annual International Conference of the IEEE Engineering in Medicine & Biology Society (EMBC)*, pages 3332–3335. IEEE, 2021. II-A
- [27] Siyuan Qiao, Liang Zhang, Xiaobo Zhang, Dacheng Tao, and Ming-Hsuan Yang. Detectors: Detecting objects with recursive feature pyramid and switchable atrous convolution. In *Proceedings of the IEEE/CVF Conference on Computer Vision and Pattern Recognition*, pages 13945–13954, 2021. III
- [28] Chaitanya Ryali, Yuan-Ting Hu, Daniel Bolya, Chen Wei, Haoqi Fan, Po-Yao Huang, Vaibhav Aggarwal, Arkabandhu Chowdhury, Omid Poursaeed, Judy Hoffman, et al. Hiera: A hierarchical vision transformer without the bells-and-whistles. In *International Conference on Machine Learning*, pages 29441–29454. PMLR, 2023. III
- [29] Ricardo Sanchez-Matilla, Maria Robu, Maria Grammatikopoulou, Imanol Luengo, and Danail Stoyanov. Data-centric multi-task surgical phase estimation with sparse scene segmentation. *International Journal of Computer Assisted Radiology and Surgery*, 17(5):953–960, 2022. II-B
- [30] Yuyang Sheng, Sophia Bano, Matthew J Clarkson, and Mobarakol Islam. Surgical-desam: decoupling sam for instrument segmentation in robotic surgery. *International Journal of Computer Assisted Radiology and Surgery*, pages 1–5, 2024. II
- [31] Zhi Tian, Tianhe He, Chunhua Shen, and Yong Yan. Conditional convolutions for instance segmentation. In *European Conference on Computer Vision*, pages 282–298. Springer, 2020. III
- [32] Thanh-Toan Vu, Changmin Yoo, and Changick Kim. Snet: Spatial context network for instance segmentation. In *Proceedings of the IEEE/CVF Conference on Computer Vision and Pattern Recognition*, pages 12032–12041, 2021. III
- [33] Chang Wang, Daming Zhang, Chao Xu, and Ming Lin. Multi-task feature aggregation for instance segmentation. In *Proceedings of the IEEE/CVF Conference on Computer Vision and Pattern Recognition*, pages 12376–12385, 2021. III
- [34] Xinlong Wang, Rufeng Zhang, Tao Kong, Lei Li, Chunhua Shen, and Yuning Jiang. Solov2: Dynamic and fast instance segmentation. In *Advances in Neural Information Processing Systems*, volume 33, pages 17721–17732, 2020. III
- [35] Qi Wu, Yuyao Zhang, and Marawan Elbatel. Self-prompting large vision models for few-shot medical image segmentation. In *MICCAI*

- workshop on domain adaptation and representation transfer*, pages 156–167. Springer, 2023. VII
- [36] Wenxi Yue, Jing Zhang, Kun Hu, Yong Xia, Jiebo Luo, and Zhiyong Wang. Surgicalsam: Efficient class promptable surgical instrument segmentation. In *Proceedings of the AAAI Conference on Artificial Intelligence*, volume 38, pages 6890–6898, 2024. VII
- [37] Yueqiang Zang, Jinglei Wu, Yunhe Wang, and et al. Fasa: Feature aggregation and selection for accurate instance segmentation. *IEEE Transactions on Medical Imaging*, 40(10):2525–2535, 2021. III
- [38] Bokai Zhang, Amer Ghanem, Alexander Simes, Henry Choi, and Andrew Yoo. Surgical workflow recognition with 3dcnn for sleeve gastrectomy. *International Journal of Computer Assisted Radiology and Surgery*, 16(11):2029–2036, 2021. II-A
- [39] Jianfeng Zhang, Bowen Cheng, Alexander Kirillov, et al. Mask dino: Masked dynamic instance normalization for end-to-end instance segmentation. In *Proceedings of the IEEE/CVF Conference on Computer Vision and Pattern Recognition*, pages 23532–23541, 2022. III
- [40] Renrui Zhang, Zhengkai Jiang, Ziyu Guo, Shilin Yan, Junting Pan, Xi-anzheng Ma, Hao Dong, Peng Gao, and Hongsheng Li. Personalize segment anything model with one shot. *arXiv preprint arXiv:2305.03048*, 2023. VII
- [41] Zixu Zhao, Yueming Jin, Xiaojie Gao, Qi Dou, and Pheng-Ann Heng. Learning motion flows for semi-supervised instrument segmentation from robotic surgical video. In *Medical Image Computing and Computer Assisted Intervention–MICCAI 2020: 23rd International Conference, Lima, Peru, October 4–8, 2020, Proceedings, Part III 23*, pages 679–689. Springer, 2020. II-B, II
- [42] Zixu Zhao, Yueming Jin, and Pheng-Ann Heng. Trasetr: track-to-segment transformer with contrastive query for instance-level instrument segmentation in robotic surgery. In *2022 International conference on robotics and automation (ICRA)*, pages 11186–11193. IEEE, 2022. II, III
- [43] Zixu Zhao, Yueming Jin, Bo Lu, Chi-Fai Ng, Qi Dou, Yun-Hui Liu, and Pheng-Ann Heng. One to many: Adaptive instrument segmentation via meta learning and dynamic online adaptation in robotic surgical video. In *2021 IEEE international conference on robotics and automation (ICRA)*, pages 13553–13559. IEEE, 2021. II-B
- [44] Aneeq Zia, Andrew Hung, Irfan Essa, and Anthony Jarc. Surgical activity recognition in robot-assisted radical prostatectomy using deep learning. In *Medical Image Computing and Computer Assisted Intervention–MICCAI 2018: 21st International Conference, Granada, Spain, September 16–20, 2018, Proceedings, Part IV 11*, pages 273–280. Springer, 2018. II-A